Physics – Uspekhi **44** (1) 53 – 70 (2001)

REVIEWS OF TOPICAL PROBLEMS PACS numbers: 42.81.Qb, 61.43.Fs, 72.20.Jv

Self-organization of excitations in Ge-doped silica fibers and its role in second harmonic generation

B P Antonyuk, V B Antonyuk

DOI: 10.1070/PU2001v044n01ABEH000867

Contents

Abstract. Based on Raman and hyper-Raman scattering experiments and on direct green light absorption measurements, excitations of a new type — charge transfer excitons — are found to exist in Ge-doped silica fibers, whose self-organization (orientation ordering of dipole moments) leads to positive feedback in response to a static electric field. An electric field of 10^5 V/cm then results breaking the inversion symmetry of the initially centrally symmetric medium and allowing the second harmonic to be generated. Generation persists only at the medium preparation stage and self-switches off upon a transition to the stationary state.

In the depths of chaos hides the miraculous.
Lao Tsu

1. Introduction

Self-organization effects in open physical systems are extremely diverse and beautiful. We will dwell briefly on some examples of such phenomena.

On mixing four or five chemical compounds (for example, sodium bromate, malonic acid, sulfuric acid, and ferroin) possessing proper correlation of densities and temperatures, the system exhibits a spontaneous self-organization into spatio – temporal dissipative structures of macroscopic dimensions. The chemical reaction produces more than 20 intermediate products. The rising chemical waves are usually followed by changes of coloring of a catalytic agent. In the two-dimensional case, the pattern quite often resembles ordered cells (honeycombs in section) or a group of concentric circles. This oscillatory system is referred to as the Zhabotinskiĭ system [1].

An effect termed Rayleigh – Benard convection provides an example of self-organization in hydrodynamics [2]. A layer of liquid (silicone oil) is sandwiched between two polished plates with a high thermal conductivity. One of the plates is heated and, if the Rayleigh number Ra (proportional to the temperature difference applied to the layer in the vertical direction) exceeds some critical value $\mathrm{Ra_c}$, a convective structure of right cylinders whose axes are perpendicular to the largest side of the base forms in the liquid layer.

The resultant periodic structure has quite a definite wavelength close, near the $\mathrm{Ra_c}$ threshold, to the doubled layer thickness. The amplitude of convection velocity $V > 0$ for $\mathrm{Ra} > \mathrm{Ra_c}$ is taken as the order parameter in the model of this phenomenon. If the Rayleigh number is below the critical one ($\mathrm{Ra} < \mathrm{Ra_c}$), the order parameter becomes equal to zero and the ordering of convective motion vanishes (a second-order phase transition).

In this connection we cannot help mentioning the Turing instability. When considering in the framework of his model the system of diffusion equations for two substances with a nonlinear right-hand side [3], A Turing concluded that a nonlinear interaction makes the stationary solution of the system unstable thus giving rise to substance density fields.

Optical morphogenesis may be regarded as the optical analog of the Turing instability. The wave equation for the electromagnetic field in a resonator in combination with the Kerr nonlinearity yields a solution in the form of a stable pattern of symmetrically alternating peaks and troughs of the intensity. This pattern is experimentally examined [4] and has nothing in common with the interference one, for it has a different spatial scale.

B P Antonyuk, V B Antonyuk Institute of Spectroscopy,
Russian Academy of Sciences,
142092 Troitsk, Moscow region, Russian Federation
Tel. (7-095) 334-02 38. Fax (7-095) 334-08 86
E-mail: antonyuk@isan.troitsk.ru; vadimant@isan.troitsk.ru

Received 20 September 2000; revised 11 October 2000
Uspekhi Fizicheskikh Nauk **171** (1) 61 – 78 (2001)
Translated by E N Ragozin; edited by A Radzig

Analyzing different examples of self-organization, I Prigogine formulated the necessary conditions for its realization (he was awarded a Nobel Prize in physics for these studies):

- the system should be open;
- the system should be essentially nonlinear;
- the self-organization should be a threshold effect, i.e. the order parameter should be nonzero when certain of the physical quantities exceed the critical values.

In 1986, the Swedish physicists Osterberg and Margulis observed a fascinating effect: a spontaneous, rather efficient (about 10%) second harmonic generation in a Ge-doped optical fiber [5]. A weak generation had been observed earlier [6]; Podobedov [7] showed later that the intensity of this generation is proportional to the surface area of the optical fiber. Owing to the violation of inversion symmetry in the near-surface layer, there is nothing to forbid the generation, and therefore a weak effect comes as no surprise. Against that, the medium is centrally symmetric in the bulk of the fiber, so that the nonlinear polarizability tensor $\chi^{(2)}$ is identically equal to zero and the frequency doubling is impossible. This is the reason why the report of highly efficient generation aroused considerable interest in this problem, and several theories were proposed.

In the first of the theories [8], attention was drawn to the fact that owing to the rectification of the fields of the first (E_1) and second (E_2) harmonics there appears a static polarization $P_0 = \chi^{(3)} E_1 E_1 E_2^*$ and the corresponding phase-matched static electric field $E_0 = -4\pi P_0$. Next it was assumed that the field E_0 orients defects and thereby a record of the spatial field distribution is brought about. It turned out, however, that the field E_0 is too weak owing to the smallness of the susceptibility $\chi^{(3)}$. The most optimistic estimates of the amplitude give $E_0 \approx 1$ V/cm, which does not of course permit the orientation of defects in a condensed medium.

Subsequent theories [9–12] proposed the idea of an asymmetric photoionization of defects under the action of the first and second harmonics. In these works, recourse was made to the free states of electrons and holes and to the multiphoton excitation of these states to describe some of the features of the phenomenon. However, a number of critical questions escaped elucidation.

In the same year of 1986, B P Antonyuk came up with the idea of self-organization of excitations with a dipole moment under the action of an intense laser field [13]. It was shown that the orientation ordering of the excitations could give rise to a strong static electric field in the medium, capable of breaking the inversion symmetry. This medium can efficiently double the frequency, and this circumstance allows us to invoke the self-organization model [13] to account for the effect of efficient second harmonic generation [5].

The optical phenomena observed in optical fibers [5] are described by the Maxwell equations or the ensuing wave equations, which should be complemented by material relationships to define the response of the medium. To this end, we need only clarify which excitations are involved in the process and describe their kinetics in the light fields present in the medium.

Osterberg and Margulis [5] employed the fundamental Nd : YAG-laser frequency ($\lambda = 1064$ nm) to obtain green light at $\lambda = 532$ nm by frequency doubling. We have pursued experiments on Raman and hyper-Raman light scattering in silica optical fibers with different GeO_2-dopant concentrations (it was precisely these optical fibers that exhibited the effect). The spectra of hyper-Raman scattering were excited by the $\lambda = 1064$ nm Nd : YAG-laser line, while the spectra of Raman scattering were excited by the line of its second harmonic ($\lambda = 532$ nm) and also by the Ar^+-laser lines at $\lambda = 514.5$ nm and $\lambda = 488$ nm.

By comparing the received spectra with the corresponding spectra of pure silicate glass, it was possible to discover a new type of excitation which occurs in the doped optical fiber but is completely absent from pure glass — a charge transfer exciton (CTE). It is significant that these states are excited by a single photon of green light.

The density dependence of the spectra obtained reveals light-driven electron transfer from a Ge-center to the matrix or to a different Ge-center when their density is high. The reverse process is attended by the emission of a luminescence photon. The corresponding CTE absorption and luminescence spectra were examined experimentally. This formed the foundation of an original model describing the self-organization of excitations in a Ge-doped silica optical fiber, which is responsible for the efficient second harmonic generation. These experiments are presented in Section 2.

It is shown in Section 3 that self-organization of CTEs (orientation ordering of their dipole moments) occurs in a laser light field, with the consequential origin of a positive feedback in response to a weak external electric field for a proper pump frequency. The CTEs are excited so that their dipole moments are primarily aligned in opposition to the field, and the resultant polarization enhances the weak external field up to 10^5 V/cm. A field like this is capable of breaking the inversion symmetry of the medium and producing efficient second harmonic generation.

In Sections 3.1 and 3.2 we consider the simplest CTE excitation model with an electron transfer to two states (along and opposite to the field) and an extended model, which permits investigation of possible electron transfers in different directions and through different distances in space. In Section 3.3 we deal with a model of independent electrons and holes, which takes into account the inhomogeneous broadening, the interaction of different Ge-centers, and the feasibility of long-range electron transfers in space. Self-organization arises in each of the three models.

In Section 4 we discuss the wave propagation of the first and second harmonics in a Ge-doped silica optical fiber, taking into account their interaction with the CTEs. Systems of four nonlinear equations for the amplitudes and the phases of the second harmonic and static polarization fields (Section 4.1) and of six equations for the amplitudes and the phases of the fields of the first and second harmonics and static polarization (Section 4.2) are derived and investigated. The former system of equations provides an adequate description of the situation where the amplitude of the second harmonic field is far less than that of the first one (such is indeed the case in the majority of experiments). The latter system of equations enables us to consider the case of arbitrary amplitudes and to estimate the conversion efficiency.

In Section 5, special emphasis is placed on the comparison of the implications of the theoretical model considered in Sections 3 and 4 with the experimental results. It is shown, in particular, that the generation is only possible at the stage of preparation and it self-terminates on passing to the stationary state, even though the strong electric field breaking the inversion symmetry persists. Subsequent to cessation of the generation, any 'shaking' of the system — be it a phase or an amplitude change of the fundamental or second harmonic

field, the imposition or the removal of a strong external electric field — results in a generation burst, which nevertheless terminates once again after a sharp rise.

The idea of a highly efficient frequency doubler based on a silica optical fiber with Ge-dopant centers is put forward. The theory developed in Sections 3 and 4 opens up possibilities for purely optical poling (polarization induction) in glasses. In media with a low carrier mobility, a light wave acts as an optical piston, which moves electrons (holes) in opposition to the force exerted on them in the static electric field, resulting in its strengthening. This amplifier of the static electric field can be employed for the poling of glasses and optical fibers in particular, which provides a possibility for producing elements of future fiber devices.

2. Experiment: a new type of excitation in Ge-doped silica optical fibers

Optical fibers, including Ge-doped ones, absorb radiation in the UV region ($\lambda < 350$ nm) and in the IR photon region ($\lambda > 2000$ nm). These optical fibers have long been thought to be transparent in the visible and near-IR ($\lambda < 2000$ nm) regions [14], and therefore the first theories [9–12] invoked the concept of multiphoton absorption at the fundamental ($\lambda = 1064$ nm) and doubled ($\lambda = 532$ nm) frequencies to account for the occurrence of second harmonic generation in the optical fibers. The free electron and hole states in silicate glasses are separated by a 'gap' of 8–10 eV, and only through the absorption of several photons can an electron be transferred from the 'valence' band to the 'conduction' band.

However, recent experiments revealed that a new type of excitation in silicate glasses appears on addition of GeO_2, which is nonexistent in pure glass as well as in GeO_2 and is excited by a single photon of green light [15–17]. The experiments on Raman and hyper-Raman scattering involved measurements of the spectra in a pure silicate glass and the corresponding spectra in a Ge-doped silica optical fiber.

The hyper-Raman spectra were excited by the fundamental frequency of Nd:YAG-laser radiation ($\lambda = 1064$ nm). The Raman spectra were observed under the excitation by the second harmonic ($\lambda = 532$ nm) as well as by the $\lambda = 514.5$ nm and $\lambda = 488$ nm Ar^+-laser lines. The light beam emerging from the optical fiber was focused on the slit of a spectrometer, which allowed the recording of the luminescence spectrum in the range up to 800 nm (a red shift $\Delta = 8000$ cm^{-1} from the excitation line at $\lambda = 488$ nm). Corrections for the variations of the spectral response of the spectrometer were introduced through a comparison with the spectrum of a band lamp with a known intensity distribution.

The hyper-Raman spectra in pure and doped glasses (Fig. 1) appear to be hardly different (only the oscillatory part is different). This is evidence that no new energy states in the doped glass come into play for irradiation at the fundamental frequency ($\lambda = 1064$ nm).

By contrast, the Raman spectra in the pure and doped glasses are significantly different. For excitation by the light with wavelengths λ_i of 488, 514.5, and 532 nm, in a Ge-doped glass a broad luminescence band appears, which is absent from pure glass (Fig. 2). The energy of the luminescent photons is about 2 eV, and the band width is 1 eV. Since the silicate glass has a large 'gap,' the luminescence band can only correspond to the electronic transitions between localized states. The 'hot' luminescence, although it could account for the width observed, is several orders of magnitude less intense owing to the fast electron relaxation (the picosecond time scale).

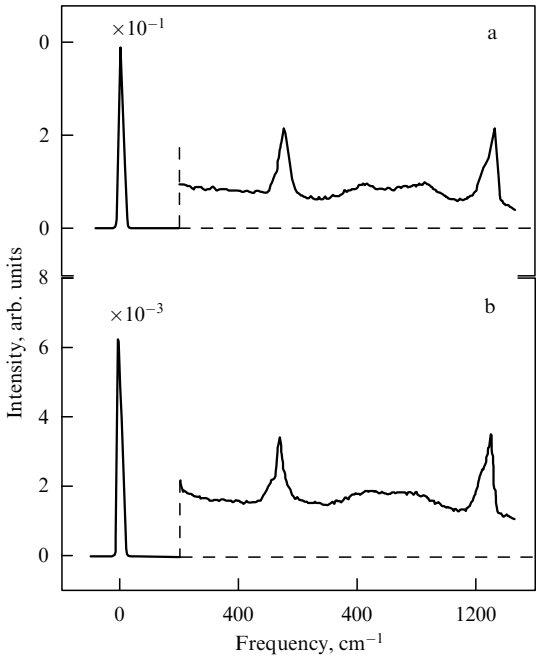

Figure 1. Hyper-Raman spectra in pure glass (a) and in a doped optical fiber (b).

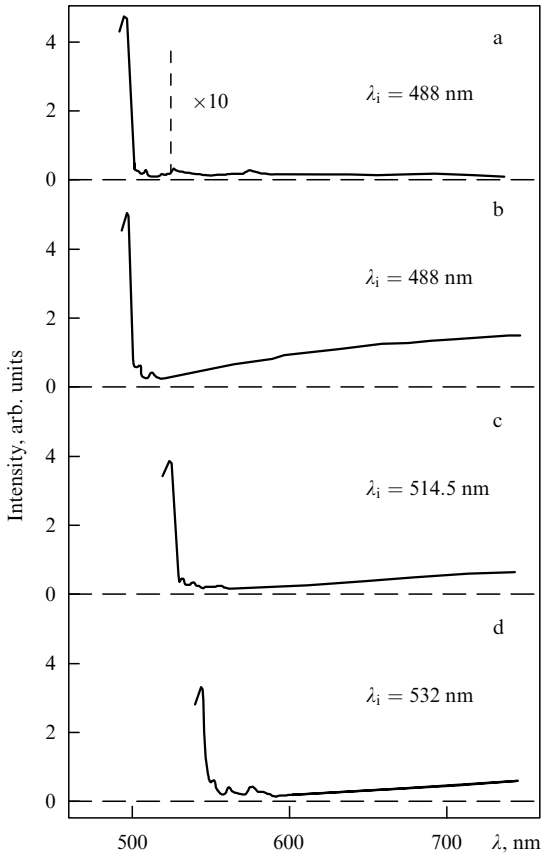

Figure 2. Raman and luminescence spectra in pure glass (a) and in a doped optical fiber (b–d) for different values of λ_i.

Electron transitions between the levels of one trap for monochromatic excitation would have given rise to discrete luminescence lines, which could be broadened by the electron–phonon interaction to $h\nu_D \sim 10^{-2}$ eV (where ν_D is the Debye frequency) but in no way to the width of 1 eV observed. That is why we attributed the broadband luminescence to transitions between different potential wells.

The observed luminescence band corresponds to a large spread of the initial electron energy values in the chaotic potential of the matrix. In the corresponding absorption event, an electron transfers from an impurity Ge-center, which serves as a donor, to a local energy well in the matrix (Fig. 3a); in this case, a CTE forms.

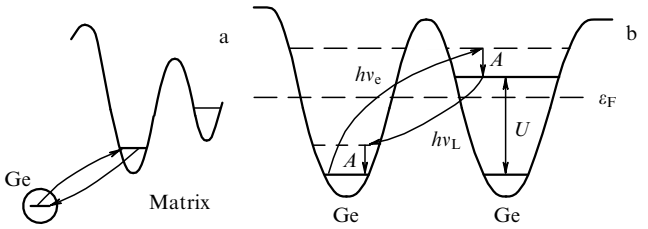

Figure 3. Electron transfer from an impurity Ge-center to the matrix (a) and between different Ge-centers (b).

We emphasize in particular that a photon of fundamental frequency ($\lambda = 1064$ nm) is insufficient to excite a CTE, which can be excited however by a single photon of the second harmonic ($\lambda = 532$ nm). In the CTE recombination, there arises a broad luminescence band, examined experimentally [15].

A more comprehensive picture of the electron transfer was obtained in studies of the concentration dependences of the spectra. The luminescence spectra were measured in the range from 488 to 740 nm in silica optical fibers with molar GeO_2-dopant concentrations of 5, 10, and 29% [16]. The spectra were normalized to the intensity of radiation emerging from the optical fiber.

The results obtained are shown in Fig. 4 in the spectral range above 523 nm. In the range below 523 nm, the luminescence spectrum is overlapped by the intense lines of Raman scattering. Referring to Fig. 4, the addition of GeO_2 gives rise to a broadband (about 1 eV) luminescence whose intensity turned out to be proportional to the pump intensity. It is therefore safe to say that the states are excited by a single photon of green light ($\lambda = 488$ nm, $h\nu_e = 2.54$ eV).

The intensity of luminescence in the $\delta\nu < 5500$ cm^{-1} (667 nm) range increases approximately linearly with the GeO_2 concentration, which is an indication that the centers involved in the emission are independent. The emission is naturally related to the electron transfers from a Ge-center to the matrix (absorption) and back (recombination with the emission of a luminescent photon).

A comparison of the spectra for low (5%) and high (10 and 29%) concentrations shows a superlinear growth of the luminescence intensity with a concentration in the $\delta\nu > 5500$ cm^{-1} range, which points to the interaction of Ge-centers. It would be natural to ascribe this radiation to the electron transfers between the Ge-centers. On excitation, an electron transfers from one Ge-center to another, recombines upon relaxation with a Stokes shift A, and next follows the second relaxation (Fig. 3b). The Coulomb electron interaction at one Ge-center, U, makes the main contribution to the excitation energy. In the ground state at each Ge-center resides one electron; in the excited state a hole is localized at one Ge-center and two electrons reside the other [16].

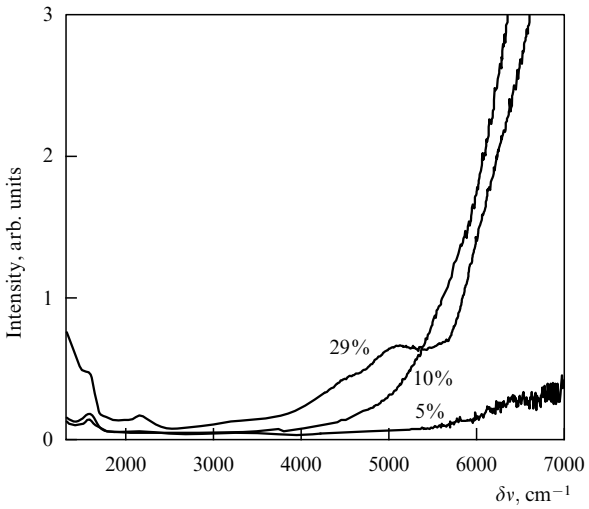

Figure 4. Luminescence spectra of an optical fiber with molar concentrations of the GeO_2 dopant of 5, 10, and 29% ($\delta\nu$ is the red shift from the $\lambda = 488$ nm exciting radiation line).

Ge-doped optical fibers exhibit low loss (about 2 dB/km) in the visible region, which cannot, despite its smallness, be attributed to the scattering alone. Clearly absorption also occurs, but it is weak and depends on the production technology of a specific optical fiber. The absorption bands are not sharply defined, and their interpretation has therefore been hampered until the present time. To elucidate this question, advantage was taken of UV irradiation as a way to act upon the absorption band. It is known that Ge-doped silica optical fibers are sensitive to UV irradiation, which permits changing the specific constituents of the absorption band.

A study was made of the absorption spectra upon irradiation by the 333, 351, and 364 nm Ar^+-laser lines [17]; in this case, oxygen-deficient centers are destroyed and different paramagnetic centers are produced [18]. These are GeE, Ge(1), and Ge(2) which absorb the UV radiation with $\lambda < 400$ nm, and nonbridged oxygen hole centers (NBOHCs) which also absorb visible light ($\lambda = 630$ nm). Also produced are diamagnetic centers which absorb the near UV and reradiate in the red region ($\lambda = 650$ nm); these are related to drawing induced defects (DID) in the production of optical fibers. The photoinduced generation or annihilation of the above defects results in a change of the refractive index and the absorption bands of the optical fiber.

Annealing at 900 °C destroys all the defects induced by UV irradiation and restores the initial state, and therefore the UV radiation can be treated as a parameter which controls selective transitions between different states of the defects. This provides the possibility of extracting specific absorption bands corresponding to different defects. Varying the GeO_2-dopant concentration or the production technology of the optical fiber leads to nonselective changes of the defect states, making measurements of the absorption bands of individual defects highly conjectural.

Studying the induced UV absorption made it possible to measure the DID ($\lambda = 438$ nm) and CTE ($\lambda = 556$ nm)

absorption bands. The absorption spectra were recorded employing an experimental facility in which the source of white light was a halogen lamp, while the detector was a monochromatizator and an FEU-100 photomultiple tube; the transmission spectra were measured over the 390–750-nm range. The Ge-doped silica core of the fiber was irradiated by the UV radiation through the output fiber face or from the side through a quartz cladding after removal of the polymer coating.

The losses induced by the 351-nm UV radiation in a 20-cm optical fiber are shown in Fig. 5. The radiation was injected into the core through a quartz lens ($F = 1$ cm), the incident power was 100 mW, and the irradiation time was 10 and 30 min. Against the background of the tail of strong short-wavelength absorption, there exist three more bands corresponding to the DID, CTE, and NBOHC absorption. The intense 630-nm band belongs to NBOHCs; for near-UV irradiation, it is observed only in optical fibers with a considerable content of the OH groups and has been studied adequately. Two close bands in the 420–600 nm range rise as the UV exposure increases.

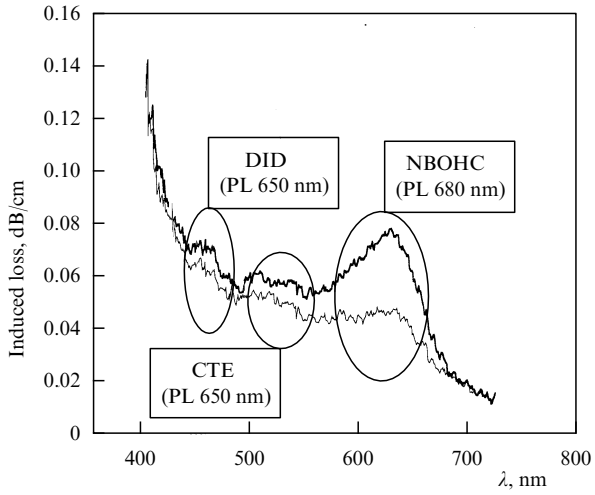

Figure 5. Induced losses in an optical fiber with a 10% molar concentration of GeO_2 upon exposure to the 351-nm UV radiation.

By exposing a 5-mm portion of the optical fiber to the 351-nm UV radiation for an incident radiation intensity of 1 kW/cm^2, two clearly defined absorption bands were obtained in the 400–600 nm range (Fig. 6). We ascribe the 438-nm band to the DID absorption, because irradiating the Ge-doped silica optical fibers with the 333, 351, 364, 458, 488, and 502-nm Ar^+-laser lines resulted in the characteristic photoluminescence at $\lambda = 650$ nm. We attribute the 556-nm absorption band to the CTE formation, for the optical fibers exhibited a broad $\lambda = 750$ nm luminescence band arising from the recombination of the above-mentioned excitons under the excitation by the 488, 502, 514, 528, and 532-nm (the second harmonic of a Nd : YAG laser) lines (see Fig. 4).

The fact that the two absorption bands in Fig. 6 belong to different defects was established in an experiment on the photodestruction of DIDs by the radiation falling within the 435-nm absorption band. A segment of the fiber was pre-irradiated by the 244-nm UV radiation (the second harmonic of the 488-nm Ar^+-laser line) with a dose of 4 J/cm^2, which resulted in the destruction of oxygen-deficient centers and the

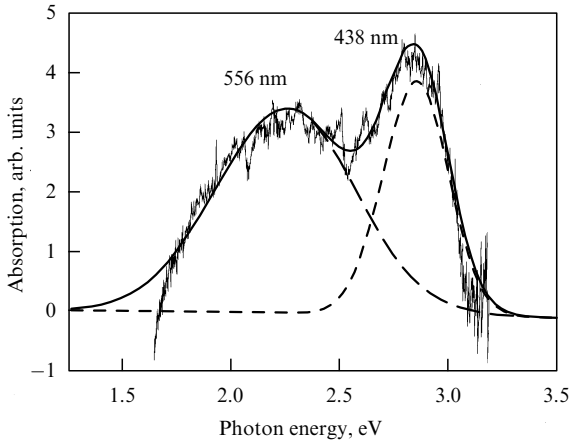

Figure 6. DID ($\lambda = 438$ nm) and CTE ($\lambda = 556$ nm) absorption bands for a 12% molar concentration of GeO_2 after exposure to the 333–364-nm UV radiation. \

DID formation. The same segment was subsequently exposed to the 364-nm UV radiation, following which there occurred a three-fold DID reduction, which obeyed an exponential law ($\tau \approx 1$ s). In this case, Ge-centers were generated, which absorbed the 556-nm band photons to form CTEs.

After the final destruction of the DIDs, the CTE absorption band gained prevalence (Fig. 7). The CTE luminescence band (see Fig. 4) was measured independently and over a broader frequency range (Fig. 8). A two-band luminescence in Fig. 8 corresponds to the two-band absorption in Fig. 6: the excitation by the 528, 458, and 488-nm lines is responsible for the luminescence of CTEs, DIDs, and their superposition, respectively [17].

Measurements of the CTE absorption and luminescence bands furnish a possibility to estimate the Coulomb interaction U of two electrons at one Ge-center and the Stokes shift A (Fig. 3b). The experimental value of the exciting photon energy is $h\nu_e = U + A \approx 2.22$ eV ($\lambda = 550$ nm) and of the luminescence photon energy $h\nu_L = U - A \approx 1.63$ eV ($\lambda = 750$ nm), whence it follows that $U = (h\nu_e + h\nu_L)/2 \approx 1.9$ eV and $A = (h\nu_e - h\nu_L)/2 \approx 0.3$ eV. Since $A \gg h\nu_D$, the case in point is a strong electron–phonon coupling characteristic of precisely the CTEs. The main contribution to their

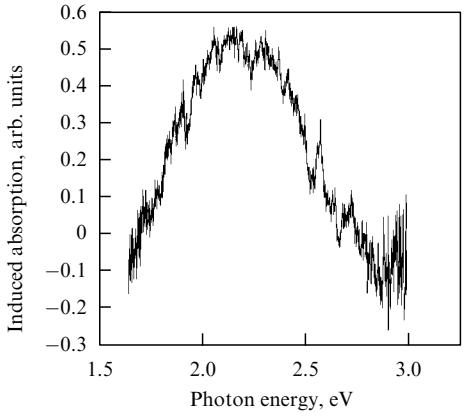

Figure 7. Induced absorption in an optical fiber with a 12% GeO_2 molar concentration, pre-irradiated by the 244-nm UV radiation, after the 364-nm UV irradiation (CTE-band formation as a result of the destruction of the DIDs).

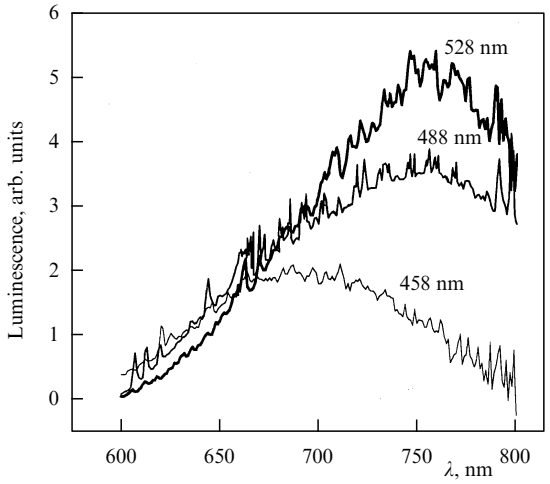

Figure 8. Strong CTE luminescence band which corresponds to the electron transfers between different Ge-centers for different wavelengths of exciting radiation ('continuation' of Fig. 4 to the $\delta\nu > 7000$ cm^{-1} range).

energy is made by the Coulomb interaction of spaced electrons and holes, which depends strongly on their separation (the derivatives of the state energy with respect to the displacements of the atoms are large).

Therefore, a number of experiments outlined in this section revealed a new type of excitation arising in a silica optical fiber on addition of a GeO_2 dopant — a charge transfer exciton. Under irradiation, the electron transfers from the impurity Ge-center to the matrix or the other Ge-center. A CTE is excited by a single photon of green light, is localized in space, and has a static dipole moment. The CTEs have come to underlie an original theoretical model for the description of second harmonic generation in Ge-doped silica optical fibers, which is discussed in the following sections.

3. Positive feedback in response to a static electric field

3.1 Response of a two-level CTE system

When considering the electron – hole kinetics in the field of a light wave, it should be remembered that there exist two types of electron – hole states in glass: free states with the wave functions covering the entire sample, and bound states with the wave functions localized in the region of potential wells. The bound-state energies are within the 'gap' between the allowed energies of free states. High-energy photons excite free electron – hole pairs, whereas low-energy photons (with energies less than the 'gap' width) give rise to transitions between localized states. Further in this section our concern will be with electron transitions from an impurity Ge-center to the matrix or to another Ge-center. The experimental examination of such transitions in absorption and luminescence spectra was outlined in the preceding section.

The experimental data allowed us to draw a conclusion that the irradiation of GeO_2-doped silicate glass gives rise to excitations of a new type, which involve spatial electron transfer (CTEs). In response to this excitation, a spatially separated localized electron – hole pair appears, which possesses a static dipole moment. The CTEs are efficiently excited by absorbing the radiation at the second-harmonic frequency, whereas the radiation at the fundamental frequency does not excite these states. The electrons localized in less deep potential wells relax fast to transfer to the deeper wells. Only these low-energy and therefore long-lived excitations play an important part in the process of self-organization. They are considered below.

The cross-section for CTE excitation and the rate of recombination at a single Ge-center are respectively

$$\sigma(\omega) = \sigma_0 \exp\left(-\frac{(2\omega - \varepsilon - A)^2}{\Delta^2} - \varkappa R\right), \qquad (3.1)$$

$$\gamma = \gamma_0 \exp(-\varkappa R).$$

Here, 2ω is the pump photon frequency, ε is the energy of phononless excitation of a CTE, A is the Stokes shift, $\Delta = 10^{-2} - 10^{-1}$ eV is the homogeneous line width, $\sigma_0 \approx 10^{-18}$ cm^2, R is the electron transfer distance, $\gamma_0 \approx 10^8$ s^{-1}, and $\varkappa \approx 5 \times 10^7$ cm^{-1}. Generally speaking, the values of ε, A, Δ, and σ_0 are different for various Ge-centers owing to inhomogeneous broadening, which is thoroughly taken into account in Section 3.3. An electron executes transfers primarily along the polarization vector of the light and in the opposite direction [13]; the probabilities of transfers in both directions are equal. The imposition of an electric field leads to its interaction with the CTE static dipole moment, and the CTE excitation energy changes by this interaction energy: $\varepsilon \to \varepsilon - \mathbf{dE}$, where $\mathbf{d}$ is the CTE static dipole moment, and $\mathbf{E}$ is the local electric field strength.

Therefore, the field splits the absorption band (3.1) for the CTEs whose dipole moment is aligned with or opposed to the applied field: $\varepsilon \to \varepsilon \pm dE$ (Fig. 9), and the transfers in one of these directions become dominant. In what direction an electron is primarily transferred with the formation of a CTE depends on the location of the exciting radiation frequency 2ω relative to the peak of the absorption band, $\varepsilon + A$.

It follows from experiments that the condition $2\omega > \varepsilon + A$ is satisfied for the second harmonic of a Nd : YAG laser and the excitations originating in a Ge-doped silica optical fiber. This implies that the CTEs with an excitation energy $\varepsilon + dE$ are closer to the exciting radiation frequency and are excited in preference. The dipole moment of these CTEs is opposed to the electric field, and the resultant polarization $\mathbf{P} = \sum \mathbf{d}$, which is also opposed to the applied field $\mathbf{E}$, leads to its

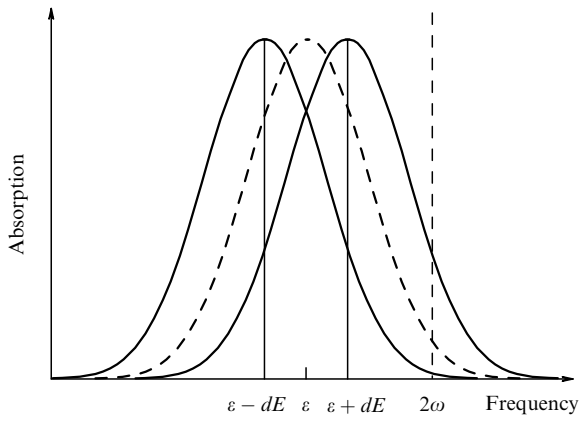

Figure 9. Splitting of the CTE absorption band in the external field E. Primarily excited are the CTEs with a dipole moment $\mathbf{d}$ opposed to the field $\mathbf{E}$; the CTE polarization strengthens the field E (positive feedback). \

strengthening. Therefore, a positive feedback is applied to the system (or a negative susceptibility): in response to the imposition of a prime electric field, the CTEs are excited not in random directions, but with dipole moments primarily oriented in such a way as to amplify this field.

We may perform a self-consistent analysis of the system response by replacing the local electric field with the macroscopic one [15]. Let ρ_+ and ρ_- be the respective probabilities that a Ge-center finds itself in the states with the dipole moments opposed to or aligned with the applied electric field **E**. Then, in the self-consistent field approximation, the rate equations for the probabilities are given by

$$\dot{\rho}_+ = I\sigma_0(1-\rho_+-\rho_-)\exp\left(-\frac{(2\omega-\varepsilon_+-A)^2}{\Delta^2}-\varkappa R\right) - \gamma_0\exp(-\varkappa R)\,\rho_+ ,$$

$$\dot{\rho}_- = I\sigma_0(1-\rho_+-\rho_-)\exp\left(-\frac{(2\omega-\varepsilon_--A)^2}{\Delta^2}-\varkappa R\right) - \gamma_0\exp(-\varkappa R)\,\rho_- ,$$

$$\varepsilon_+ = \varepsilon + dE, \quad \varepsilon_- = \varepsilon - dE, \quad \mathbf{E} = \mathbf{E}_\mathrm{i} - 4\pi q\mathbf{P},$$

$$\mathbf{P} = \alpha\mathbf{E} + n\langle\mathbf{d}\rangle, \quad \langle\mathbf{d}\rangle = \mathbf{d}\,(\rho_- - \rho_+). \tag{3.2}$$

Here, I is the pump intensity, ε_+ and ε_- are the energies of the CTEs in the two states, **E** is the macroscopic electric field strength which is the sum of the initial field $\mathbf{E}_\mathrm{i}$ and the polarization addition, $-4\pi q\mathbf{P}$, the polarization **P** includes the linear constituent $\alpha\mathbf{E}$ (α is the medium susceptibility) and the nonlinear CTE polarization $n\langle\mathbf{d}\rangle$, **d** is the CTE dipole moment, n is the CTE concentration, and q is the geometric factor: $q = 1$ for a plane geometry, $q = 1/2$ for a cylindrical geometry, and $q = 1/3$ for a sphere [19].

The priority population of the '+' state with the dipole moment in opposition to the field **E** and having a higher energy, corresponds to a positive feedback. The thermodynamic population of the '−' state, which possesses a lower energy (the dipole moment is aligned with the field), is always stronger ($\rho_- > \rho_+$), which corresponds to a negative feedback in full accord with the Le Chatelier principle which holds good for closed systems. The Le Chatelier principle cannot be extended to an open system (such is the case for the system under investigation, exposed to an external light field), and its response may be any one of these.

The stationary solution (3.2) is easy to find graphically, especially for the case $\rho_+, \rho_- \ll 1$. In fact, for $\dot{\rho}_+ = \dot{\rho}_- = 0$ we have

$$\rho_+ = \frac{I\sigma_0}{\gamma_0}\exp\left(-\frac{(2\omega-A-\varepsilon-\bar{d}\bar{E})^2}{\Delta^2}\right),$$

$$\rho_- = \frac{I\sigma_0}{\gamma_0}\exp\left(-\frac{(2\omega-A-\varepsilon+\bar{d}\bar{E})^2}{\Delta^2}\right).$$

Furthermore, we calculate the average dipole moment and the polarization using formulas (3.2) to obtain the transcendental equation for the electric field **E**:

$$\bar{E} = \frac{\bar{E}_\mathrm{i}}{1+4\pi q\alpha} + \frac{4\pi qnI\sigma_0 d}{(1+4\pi q\alpha)\gamma_0}\left[\exp\left(-\frac{(2\omega-A-\varepsilon-\bar{d}\bar{E})^2}{\Delta^2}\right) - \exp\left(-\frac{(2\omega-A-\varepsilon+\bar{d}\bar{E})^2}{\Delta^2}\right)\right]. \tag{3.3}$$

The graphic solution (3.3) shows the existence of the above-mentioned positive feedback and the bistability in the dependence $E(E_0)$.

The result of numerical solution to the system of equations (3.2) is given in Fig. 10. The ground state ($\rho_+ = \rho_- = 0$) was taken as the initial conditions, next pursued was the asymptotic state of the system for long times. This approach automatically provides the answer to the question of stability: only stable states can be reached. The following parameters were introduced to go over to dimensionless variables:

$$\xi = \frac{2\omega-\varepsilon-A}{\Delta}, \quad \mu = \frac{I\sigma_0}{\gamma_0}, \quad \widetilde{E} = \frac{dE}{\Delta},$$

$$\widetilde{E}_\mathrm{i} = \frac{dE_\mathrm{i}}{(1+4\pi q\alpha)\Delta}, \quad g = \frac{4\pi qnd^2}{(1+4\pi q\alpha)\Delta}, \quad \tau = \gamma_0 t. \tag{3.4}$$

The transition of the system to a self-ordered state was considered for an intense pumping ($\mu = 1$), which corresponds to a value of $I \approx 4\times10^7$ W/cm^2.

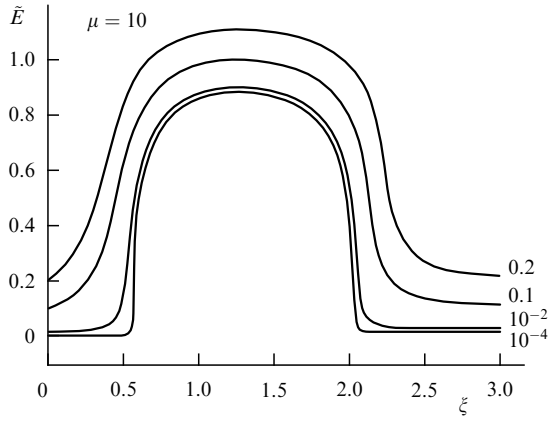

Figure 10. Resultant static field $\widetilde{E}$ as a function of the frequency of exciting radiation for different intensities of the prime field $\widetilde{E}_\mathrm{i}$.

Therefore, irrespective of the intensity of the initial field $\widetilde{E}_\mathrm{i}$ within a specific frequency range, the system polarizes in opposition to the field in such a way that the dimensionless resultant field, strengthened by the polarization, attains a magnitude $\widetilde{E} \approx 1$, which corresponds to a physical field $E \approx 10^5$ V/cm. As regards other parameters of the problem, we put $d = 5\times10^{-18}$esu, and $\Delta = 10^{-2}-10^{-1}$ eV. Since the amplifying polarization addition is independent of the initial field $\widetilde{E}_\mathrm{i}$ over a broad range of values $\widetilde{E}_\mathrm{i} \approx 10^{-4}-2\times10^{-1}$, the initial field affects only the polarization direction and its magnitude depends on the intrinsic system properties. In this particular case, the self-organization involves the ordering of the CTE dipole moments in the field of a light wave (orientation ordering).

3.2 Response of a CTE system with distant electron transfers

The CTE excitation model with electron transfer in two directions by a fixed distance in space allows one to depict a qualitative picture of self-organization and the corresponding positive feedback and to estimate the order of magnitude of the amplified resultant field. The extended model, in which a study is made of possible electron transfers in different directions and by different distances in space, is outlined

below [20]. This model enables us to estimate the particular role of distant transfers, which are responsible for long-lived excitations, and the effect of pump intensity on the occurrence of self-organization in the system.

Let an electron transfer under the action of pump from an impurity Ge-center to the matrix, and let R_m be the transfer distance, and d_m the corresponding dipole moment. The CTE excitation cross-section and the recombination rate are described by formulas (3.1), while the system of kinetic equations (3.2) for two possible excited states assumes the form

$$\dot{\rho}_m = I\sigma_0\Big(1-\sum_l \rho_l\Big)\cos^2\theta_m \times \exp\left(-\frac{(2\omega-\varepsilon_m-A)^2}{\Delta^2}-\varkappa R_m\right)-\gamma_0\exp\left(-\varkappa R_m\right)\rho_m\,, \tag{3.5}$$

$$\varepsilon_m = \varepsilon - \mathbf{d}_m\mathbf{E}\,,\quad \mathbf{E}=\mathbf{E}_{\rm i}-4\pi q\mathbf{P}\,,$$
$$\mathbf{P}=\alpha\mathbf{E}+n\langle\mathbf{d}\rangle\,,\quad \langle\mathbf{d}\rangle=\sum_m \mathbf{d}_m\rho_m\,,$$

where ρ_m is the probability of a Ge-center occurring in the excited state m, θ_m is the angle between the direction $\mathbf{R}_m$ of electron transfer and the vector of light polarization, and ε_m is the energy of the phononless excitation of a CTE in the external electric field $\mathbf{E}$; the matrix is treated as a cubic lattice (a is the lattice constant, so that $\varkappa = 1/a$).

We found the numerical solution of the system of equations (3.5) for the possible electron transfers from a Ge-center to any point $m=(m_1,m_2,m_3)$ of a cubic lattice, up to the maximum transfer distance $R^2 \geqslant m_1^2+m_2^2+m_3^2$, which was assumed to vary within the range $R=1-7$. The passage to dimensionless variables was accomplished employing formulas (3.4).

It turned out that the resultant electric field $\widetilde{E}$ is, like in the model considered in Section 3.1, independent of the initial field $\widetilde{E}_{\rm i}$. The dependence of the field on the pump frequency (for asymptotically long times) is plotted in Fig. 11 for different maximum transfer distances R. These results were obtained for a weak pump ($\mu = 0.01$).

One can see from the results outlined that the strengthening of the initial field occurs for any pump if long-distance electron transfers are engaged. The probability w_m of the electron transfer to a point m decays exponentially with transfer distance: $w_m \propto \exp(-\varkappa R_m)$. Nevertheless, the fast decay of the population probability with the transfer distance R_m does not signify that the role of the states with a large electron-transfer distance is small. The rate of decay of an excited CTE, $\gamma_m = \gamma_0\exp(-\varkappa R_m)$, is proportional to the same exponential factor, and the steady-state probability that an electron is found in an excited state m is independent of the transfer distance R_m. The states with a longer transfer distance are more slowly pumped but have longer lifetimes; upon termination of the pump, the states with a short transfer distance therefore relax rapidly and only the states with a longer transfer distance survive. These states possess a larger static dipole moment and play a greater part in the self-organization of CTEs.

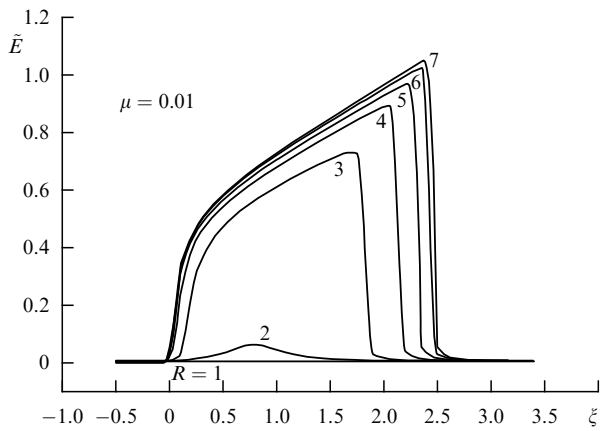

Figure 11. Resultant static field $\widetilde{E}$ as a function of the frequency of exciting radiation for different values of the maximum transfer distance R.

The larger the distance of electron transfer, the longer the time required to populate this state: $t \propto \exp(\varkappa R_m)$. Hence, the longer the experiment duration, the weaker may be the pump which gives rise to the CTE self-organization leading to second harmonic generation. In the first experiment [5], the initially weak second harmonic resulted in self-organization after five hours of irradiation. The self-organization typically has a threshold, but the threshold tends to zero as the time of preparation of the state increases.

3.3 Response of localized electrons and holes

The most general microscopic model, which allows the inhomogeneous broadening and the possibility of distant electron transfers in space to be taken into account, is the model of independent electrons and holes outlined below [21].

The probability w_{ij} that an electron transfers from a trap i to a trap j on pumping assumes the form

$$w_{ij} = I\sigma_0\cos^2\theta_{ij}\exp\left(-\frac{(2\omega-\varepsilon_{ij}-A)^2}{\Delta^2}-\varkappa_{ij}R_{ij}\right), \tag{3.6}$$

where θ_{ij} is the angle between $\mathbf{R}_{ij}$ and the light polarization vector, the factor $\varkappa_{ij}$ is determined by the degree of overlapping of the wave functions of the initial and final states and depends on the corresponding energies ε_i and ε_j. The probability (3.6) decays exponentially with transfer distance $|\mathbf{R}_{ij}| = |\mathbf{R}_j - \mathbf{R}_i|$ and passes through a resonance for $2\omega = \varepsilon_{ij} + A$, where $\varepsilon_{ij} = \varepsilon_j - \varepsilon_i$ and A is the Stokes shift. The wave functions of the electrons residing in deep energy levels decay fast as they recede from the localization region; the wave functions of the electrons with higher energies decay more slowly.

The wave function of an electron localized in a trap i, obtained in the solution of the Schrödinger equation, decays with distance outside of the potential well according to the following formula

$$|i\rangle = \sqrt{\varkappa_i}\exp\left(-\varkappa_i|\mathbf{R}-\mathbf{R}_i|\right), \tag{3.7}$$

where

$$\varkappa_i = \sqrt{\frac{2m}{\hbar^2}(V-\varepsilon_i)} = \varkappa_0\sqrt{1-\frac{\varepsilon_i}{V}},$$

V is the spacing of the Fermi level from the edge of the forbidden band, and ε_i is the energy of the state relative to the Fermi level. Although doped glasses are not a thermodynamically equilibrium medium and the Fermi level is not, strictly speaking, defined for them, we will introduce it in

the usual way to describe a partial equilibrium. By a Fermi level is meant an energy level above which the electron states are not occupied, and it is assumed to lie in the middle of the forbidden band. Therefore, the forbidden gap width is $2V \approx 8$ eV, and we obtain a quantitative estimate of $\varkappa_0$ in the following way: $\varkappa_0 = (2m/\hbar^2 V)^{1/2} \approx 2 \times 10^{-7}$ cm^{-1}.

The $|i\rangle$-to-$|j\rangle$ transition matrix element, which leads to the probability formula (3.6), includes the overlap integral of the wave functions of the initial and final states, equal to

$$\langle i\,|\,j\rangle = \frac{\sqrt{\varkappa_i \varkappa_j}}{\varkappa_i + \varkappa_j} \exp\left(-\varkappa_i R_{ij}\right) + \frac{\sqrt{\varkappa_i \varkappa_j}}{\varkappa_i - \varkappa_j}\left[\exp\left(-\varkappa_j R_{ij}\right) - \exp\left(-\varkappa_i R_{ij}\right)\right] + \frac{\sqrt{\varkappa_i \varkappa_j}}{\varkappa_i + \varkappa_j} \exp\left(-\varkappa_j R_{ij}\right). \tag{3.8}$$

Since the integral (3.8) decreases steeply with distance, the sum will be dominated by the terms corresponding to the more slowly decaying exponent, i.e. it can be assumed that $\varkappa_{ij} = \min\{\varkappa_i, \varkappa_j\}$ with an exponential accuracy. In this approximation, $\varkappa_{ij}$ is the decay distance of the wave function of the highest-energy particle. The wave function of such a particle falls off slowly, and it is precisely this function that determines the matrix element (3.8).

The electron energy ε_i depends on the spatial distribution of the surrounding electrons and holes and is determined by the Coulomb interaction:

$$\varepsilon_i = \varepsilon_i^{(0)} + \sum_m^{(\mathrm{e})} \frac{e^2}{R_{im}} - \sum_m^{(\mathrm{h})} \frac{e^2}{R_{im}}, \tag{3.9}$$

where the sums $\sum_m^{(\mathrm{e})}$ and $\sum_m^{(\mathrm{h})}$ are taken over the already excited electron and hole states, respectively, and $\varepsilon_i^{(0)}$ is the electron energy level of the trap in the ground state.

Apart from radiation-induced electron transitions with a gain in energy, which are determined by formula (3.6), there exist transitions with a loss in energy. Their probability is defined by that same formula (3.6), though with a replacement $A \to -A$. Also possible are the $i \to j$ spontaneous transitions with an energy lowering (recombination, when the electron crosses the Fermi level, and relaxation otherwise). These transitions may be divided into two types [22]: radiative transitions, in which the energy difference is carried away by the photon, with the decay rate

$$\gamma_{ij} = \gamma_0 \exp\left(-\varkappa_{ij} R_{ij}\right), \tag{3.10}$$

and the phonon ones, whose decay rate is determined by the energy $|\varepsilon_{ij}| = |\varepsilon_j - \varepsilon_i|$ transferred into phonon oscillations:

$$\Gamma_{ij} = \gamma_1 \exp\left(-\varkappa_{ij} R_{ij} - \frac{|\varepsilon_{ij}|}{\hbar\omega_{\mathrm{D}}}\right). \tag{3.11}$$

Formula (3.11) takes into account that the phonon transition probability decreases exponentially with the number of phonons participating in the process, i.e. with the energy difference between the initial and final states. The factors γ_0 and γ_1 can be estimated from experiments: for short-distance transfers, the decay rate γ_{ij} should be of the order of magnitude of the inverse lifetime for excited electron states in an atom, and the decay rate Γ_{ij} is equal to the intermolecular relaxation rate, which gives $\gamma_0 \approx 10^8$ s^{-1} and $\gamma_1 \approx 10^{12}$ s^{-1}.

The experiments discussed in Section 2 showed that the system of potential wells (traps) in a Ge-doped silica optical fiber can be described in the framework of the following model. Initially, a trap in the matrix has one electron level $\varepsilon_i^{(0)}$, whereas a Ge-center may be occupied by one electron (energy of state $\varepsilon_i^{(0)}$) or two electrons (energy of state $2\varepsilon_i^{(0)} + U$, where U is the energy of Coulomb electron interaction). We observed both a linear dependence of the luminescence on the concentration of Ge-centers, which corresponds to the Ge-center – matrix electron transitions, and a superlinear one, which corresponds to the Ge-center – Ge-center transitions (Fig. 3b).

The traps in the matrix and the Ge-centers are randomly distributed over the volume of the sample and their initial energy levels $\varepsilon_i^{(0)}$ are also randomly distributed in accordance with the densities of states $\rho(\varepsilon_i^{(0)})$. We studied various Ge-center concentrations and Gaussian probability densities $\rho(\varepsilon_i^{(0)})$ with different variances Δ_{Ge}. The computation commenced with the ground state, where all the electron levels below the Fermi energy ($\varepsilon_i^{(0)} < 0$) are occupied and the levels with $\varepsilon_i^{(0)} > 0$ are free. Computer simulation of the electron – hole kinetics was performed taking into account the formulas for transition probabilities (3.6), (3.10), and (3.11); at each time step the electron energy (3.9) was calculated as was the exponential factor $\varkappa_{ij}(\varepsilon_i^{(0)}, \varepsilon_j^{(0)})$ defined by formula (3.7). We investigated the time dependence of the polarization $\mathbf{P}(t)$ of the sample for different intensities of the external field $\mathbf{E}_0$, the pump intensity I, and the parameters of the medium. The dimensionless parameters of the problem took the form

$$\tau = \gamma_0 t, \quad r = \frac{R}{a}, \quad \mu = \frac{I\sigma_0}{\gamma_0}, \quad Q = \frac{e^2}{a\Delta}, \quad \widetilde{E} = \frac{Eea}{\Delta}$$

for an average spacing between the traps $a \approx 5 \times 10^{-8}$ cm. The volume of the sample was defined as $V = Na^3$, where $N = N_1 N_2 N_3$ is the total number of traps. The polarization of the sample

$$\mathbf{P} = \frac{1}{V}\left(\sum_j^{(\mathrm{h})} |e|\mathbf{R}_j - \sum_i^{(\mathrm{e})} |e|\mathbf{R}_i\right), \tag{3.12}$$

was measured in the units $|e|/a^2 = 2 \times 10^5$ esu $= 64$ μC/cm^2; the sums $\sum_m^{(\mathrm{e})}$ and $\sum_m^{(\mathrm{h})}$ in expression (3.12) were taken over the excited electron and hole states.

The relaxation and recombination [both for photons as determined by Eqn (3.10), and phonons by Eqn (3.11)] are responsible for the usual mobility in the direction of the acting force $e\mathbf{E}_0$, which forms a polarization $\mathbf{P}$ aligned with the external field $\mathbf{E}_0$ (a normal negative feedback which weakens the field $\mathbf{E}_0$). Light can transfer electrons in a direction opposite to the acting force. We observed the competition of these two processes for different external parameters ($\mathbf{E}_0$, I, ω) and matrix parameters. In the case of a low electron (hole) mobility, the light-induced transfers prevail and the resultant polarization $\mathbf{P}$ is opposed to the external field $\mathbf{E}_0$, which leads to its strengthening (a positive feedback). For molar concentrations higher than 10%, the transitions between the Ge-centers prevail and the matrix is not active (the electron-state density in the traps of the matrix in the vicinity of the Fermi energy is low) [16].

A study was made of the Gaussian distribution of the Ge-center electron energy levels $\varepsilon_i^{(0)}$ with variances Δ_{Ge} located below the Fermi level, with the second electron level of the

impurity center with an energy $\varepsilon_i^{(0)} + U > 0$ being above the Fermi level. This study showed that transitions to the free states with energies $\varepsilon_i^{(0)} + U$, which also have a Gaussian density distribution, are possible. A positive feedback in response to an external static field is observed in a system of this kind (Fig. 12).

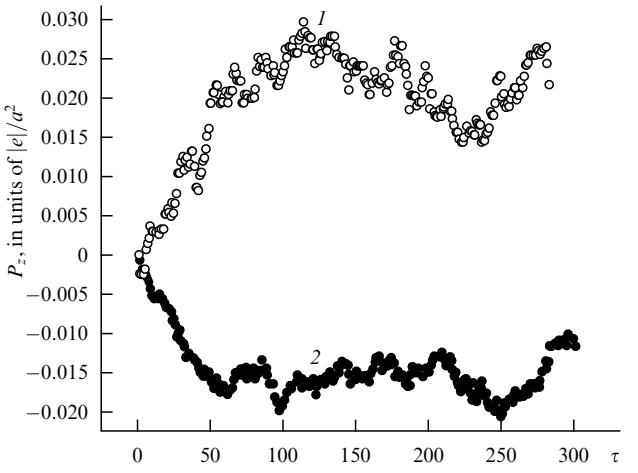

Figure 12. Time dependence of the sample polarization in the z-direction (along the external field) for the model of electron transfers between the Ge-centers. Curve *1* corresponds to the parameter values $\widetilde{E}_0 = -0.25$, $\mu = 10^{-3}$, $a = 2.5$ nm, $1/\varkappa = 0.1$ nm^{-1}, $\Delta_{\mathrm{Ge}} = 1.5$ eV, $U_0 = -1$ eV, $U = 2$ eV, $\hbar\omega = 2.5$ eV, $\gamma_{\perp} = 0$, and the sample measures $6 \times 6 \times 60$. Curve *2*: the same, except that $\widetilde{E}_0 = 2.5$ and the sample measures $6 \times 60 \times 6$.

An electric field strength $\mathbf{E} = -4\pi q\mathbf{P} \approx 10^6$ V/cm corresponds to a dimensionless polarization $\mathbf{P} \approx 10^{-2}$. The reason why the light-induced transfers occur in the direction opposite to the acting force can be qualitatively understood. In this case, the electron-state density in the vicinity of the Fermi level is vanishingly low and the usual electron mobility along the direction of the external force $e\mathbf{E}_0$ is missing. The required mobility only arises in the excited state and is determined by the excited-particle density. For low densities, the mobility is low and the light-induced transitions from the ground state prevail. These are precisely the ones which produce a positive feedback.

A positive feedback takes place for a broad class of materials with a low mobility of electrons and holes, including systems with a nonzero density of states in the vicinity of the Fermi level. Examples of such behavior for an inhomogeneously broadened local level are given in Fig. 13. The above-mentioned polarization orientation in opposition to an external field is demonstrated in Figs 12 and 13. Calculations for $\gamma_1 = 10\,\gamma_0$ do not qualitatively change the observed picture. Also noteworthy is the existence of strong fluctuations exceeding the regular magnitude $N^{-1/2}$. The details of the calculations are given elsewhere [21, 23, 24].

Therefore, a consideration of the simplest, extended, and general models which describe the kinetics of electrons and holes showed that the self-organization of excitations leads to the occurrence of positive feedback in response to an external static electric field: a polarization is induced, which strengthens the weak external field up to $10^5 - 10^6$ V/cm. The strong static electric field resulting from the application of positive feedback breaks the inversion symmetry of the medium and makes possible an efficient second harmonic generation.

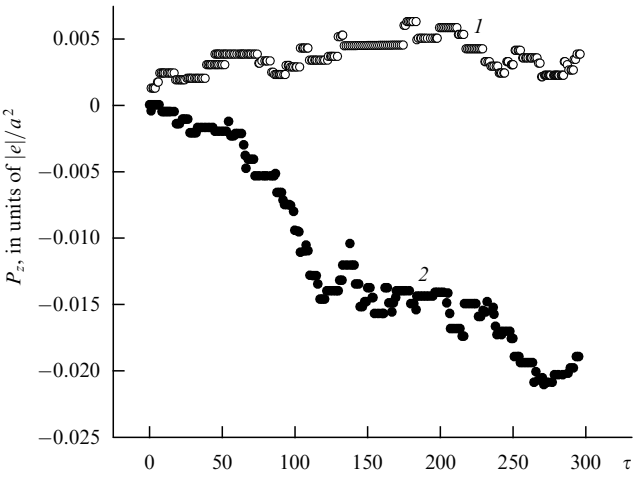

Figure 13. Time dependence of the sample polarization in the z-direction for the model of electron transfers between the traps in the matrix. Curve *1* corresponds to the parameter values $\rho(\varepsilon_i^{(0)}) = \exp\left[-(\varepsilon_i^{(0)}/\sqrt{2}\Delta)^2\right]$, $\widetilde{E}_0 = -0.25$, $\mu = 10^{-3}$, $a = 2.5$ nm, $1/\varkappa = 0.1$ nm^{-1}, $\Delta = 4.5$ eV, $\hbar\omega = 2.4$ eV, $\gamma_{\perp} = 0$, and the sample measures $6 \times 60 \times 6$. Curve *2*: the same, except that $\widetilde{E}_0 = 0.2$, $a = 2.0$ nm, and the sample measures $8 \times 80 \times 8$.

4. Wave propagation through a Ge-doped silica optical fiber

4.1 Propagation of a weak second-harmonic wave

The second-harmonic wave propagation through a Ge-doped silica optical fiber is described by a wave equation with a specific nonlinear right-hand side:

$$\frac{n_{2\omega}^2}{c^2}\,\frac{\partial^2 E}{\partial t^2} - \frac{\partial^2 E}{\partial z^2} = -\frac{4\pi}{c^2}\,\frac{\partial^2 P_{\mathrm{NL}}}{\partial t^2}\,. \tag{4.1}$$

It is common for the amplitude of the second harmonic to be two orders of magnitude smaller than that of the fundamental wave. In this situation it is valid to neglect the nonlinear variations of the latter and consider the variation of the second harmonic alone [25].

We write down the electric field intensities for the fundamental wave and the sought second harmonic:

$$E_\omega = A_1(z)\exp\left[\mathrm{i}k_\omega z - \mathrm{i}\omega t\right],$$

$$E_{2\omega} = A_2(z)\exp\left[\mathrm{i}k_{2\omega}z - 2\mathrm{i}\omega t + \mathrm{i}\psi_2(z)\right],$$

where the amplitude $A_2(z)$ and the phase $\psi_2(z)$ are real and slowly varying variables. We substitute the expression for the second harmonic into Eqn (4.1) and write down the nonlinear polarization at the doubled frequency in the form

$$P_{\mathrm{NL}} = P_{2\omega}\exp\left[\mathrm{i}k_{2\omega}z - 2\mathrm{i}\omega t\right],$$

to obtain the equation for the complex amplitude of the second harmonic:

$$\frac{\partial}{\partial z}\left[A_2\exp\left(\mathrm{i}\psi_2\right)\right] = \mathrm{i}\frac{4\pi\omega}{cn_{2\omega}}\,P_{2\omega}\,, \tag{4.2}$$

where $n_{2\omega}$ is the refractive index at the doubled frequency.

To arrive at a closed system, the wave equation and the ensuing equation for the complex amplitude of the second-harmonic field (4.2) should be supplemented with the

equations describing the response of the medium. The polarization $P_{2\omega}$ at the doubled frequency arises due to the nonlinear polarizability tensor $\chi^{(3)}$ in the presence of a strong static field: $P_{2\omega} = \chi^{(3)} E_{\rm dc} E_{\omega}^2$.

Let us consider the mechanism of the origin of a strong static field $E_{\rm dc}$. The fundamental wave and the second-harmonic wave produce a fast nonlinear polarization in the medium:

$$P_{\rm dc}^{(0)} = \chi^{(3)} A_2 A_1^2 \exp\left[\mathrm{i}(k_{2\omega} - 2k_{\omega})z + \mathrm{i}\psi_2\right].$$

The electric field $E_{\rm dc}^{(0)} = -4\pi q P_{\rm dc}^{(0)}$ resulting from the 'rectification' has a small amplitude (about 1 V/cm) but satisfies the phase-matching condition required for the efficient generation of the second harmonic and is the necessary 'seed' when acting on the slow system of CTEs. In response to the pump, the CTEs strengthen the prime ('seed') field and retain its direction in space, i.e. the phase (the amplification mechanism was considered in Section 3).

The resultant static field tends to saturation:

$$E_{\rm dc} \to -u \exp\left[\mathrm{i}(k_{2\omega} - 2k_{\omega})z + \mathrm{i}\psi_2\right],$$

where the amplitude $u \approx \Delta/d \approx 10^5$ V/cm (for more details, see Section 3). The amplified static field breaks the inversion symmetry and results in frequency doubling through the occurrence of effective nonlinear second-order susceptibility $\chi^{(2)}(z) = \chi^{(3)} E_{\rm dc}(z)$. According to the experimental data, an CTE is excited by one second-harmonic photon, and therefore the rate with which the static field $E_{\rm dc}$ tends to saturation is proportional to the power of the second harmonic and is equal to $\alpha_2 A_2^2$, where α_2 is the proportionality coefficient.

We will seek the solution for $E_{\rm dc}$ in the form

$$E_{\rm dc}(z,t) = -A_0(z,t) \exp\left[\mathrm{i}(k_{2\omega} - 2k_{\omega})z + \mathrm{i}\psi_0\right].$$

Simulations show that $E_{\rm dc}$ tends exponentially to the stationary value, in accordance with the equation

$$\frac{\partial}{\partial t} A_0\left[\exp(\mathrm{i}\psi_0)\right] = \alpha_2 A_2^2 \left[u \exp(\mathrm{i}\psi_2) - A_0 \exp(\mathrm{i}\psi_0)\right]. \quad (4.3)$$

Equations (4.2) and (4.3) furnish a complete evolutionary description of the amplitude and the phase of the second-harmonic wave and of the static field in the case where the amplitude of the second-harmonic field is significantly lower than that of the fundamental one.

By going over to dimensionless variables with the use of the formulas

$$E_0 = \frac{A_0}{u}, \quad E_2 = \frac{A_2}{u}, \quad S = \varkappa_0 z,$$
$$\varkappa_0 = \frac{4\pi\omega\chi^{(3)}A_1^2}{c n_{2\omega}}, \quad \tau = \alpha_2 u^2 t \quad (4.4)$$

and separating the amplitudes and the phases in Eqns (4.2) and (4.3), we obtain a universal system of four equations, which retains all the properties of Eqns (4.2) and (4.3) but is more advantageous for the future investigation:

$$\begin{aligned}
&\frac{\partial E_2}{\partial S} = E_0 \sin(\psi_0 - \psi_2), \\
&E_2 \frac{\partial \psi_2}{\partial S} = -E_0 \cos(\psi_0 - \psi_2), \\
&\frac{\partial E_0}{\partial \tau} = -E_2^2\left[E_0 - \cos(\psi_0 - \psi_2)\right], \\
&E_0 \frac{\partial \psi_0}{\partial \tau} = -E_2^2 \sin(\psi_0 - \psi_2).
\end{aligned} \quad (4.5)$$

The system of equations (4.5) is remarkable for the absence of parameters: all of them enter into the scaling factors of the quantities (4.4). The formulas for going over to the dimensionless variables (4.4) allow one to estimate the scales of the variables that enter Eqns (4.5): the unit of electric field intensity $u \approx 10^5$ V/cm, the unit of length $\varkappa_0^{-1} \approx 10$ cm, and the unit of time is $(\alpha_2 u^2)^{-1}$. This yields for the time scale $(\alpha_2 u^2)^{-1} \approx 5$ min, in accordance with the experimental time taken to prepare the state by the second harmonic with an amplitude approximately equal to u [8].

It is easily seen that the system of equations (4.5) has a stationary solution:

$$\psi_0 = \psi_2, \quad E_0 = 1, \quad E_2 = \text{const},$$

i.e. there exists a static electric field but there is no second harmonic generation. Therefore, the second harmonic generation is only possible in the preparation stage, when the static polarization field has not yet reached the saturation value and there exists a phase difference $\psi_0 - \psi_2 \neq 0$. This phase difference arises owing to the delay time characteristic of the system for $E_2 \ll 1$ (the static polarization forms over a long time period). In this situation, the amplitude of the second harmonic varies along the optical fiber.

As the amplitude of the second harmonic increases ($E_2 \approx 1$), the delay time decreases, and the phase of the static field more closely follows the phase of the second-harmonic field ($\psi_0 - \psi_2 \to 0$). As a consequence, as is seen from Eqns (4.5), the system seeks the stationary state, which is, however, trivial in nature: only the phase of the second harmonic varies while its amplitude remains invariable through the optical fiber. The second harmonic generation therefore possesses the property of self-switching off.

Plotted in Fig. 14 is the numerical solution of the system (4.5) for the initial values of the static field $E_0(0,S) = 0$, $\psi_0(0,S) = 0$ and the second-harmonic field $E_2(\tau,0) = 0.05$, $\psi_2(\tau,0) = 0$ (which corresponds to the experiment with the 'prime' wave [8]). One can see from the plot that the delay time (the phase difference) tends to zero and the growth of the second harmonic terminates as its amplitude builds up. From this point on only the rotation of the complex amplitude of the second harmonic occurs. The saturation length is in order

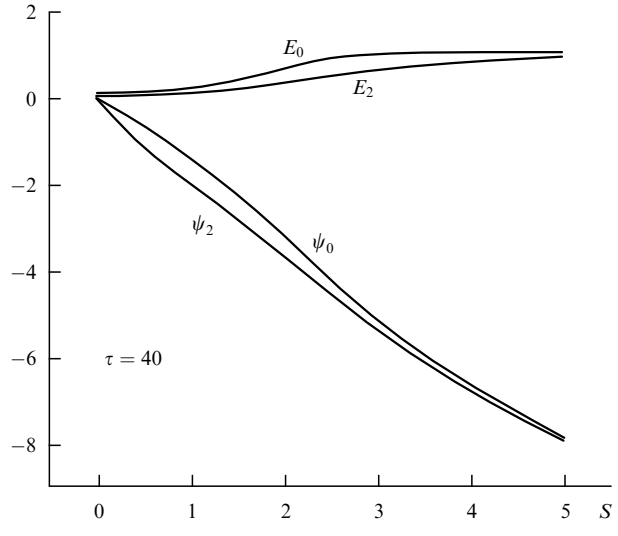

Figure 14. Spatial distribution of the amplitudes and phases of the second-harmonic and static-polarization fields.

of magnitude equal to $\varkappa_0^{-1} \approx 10$ cm, and a further increase in the optical fiber length does not result in an increase of the second-harmonic signal.

The time dependence of the output second-harmonic signal is shown in Fig. 15 for a length $S = 5$. The plots are given for different values of the second-harmonic prime wave: from a weak wave $[E_2(\tau, 0) = 0.05]$ to a very strong one $[E_2(\tau, 0) = 1.2]$. The fast growth of the second-harmonic amplitude (which is faster, the higher the intensity of the input signal) and a slower subsequent decline to the initial value are evident. Figure 16 shows the picture of second harmonic generation. The stage of state preparation, where the generation takes place, and the asymptotic (prepared) state, where $E_0(\tau, S) \to 1$, $E_2(\tau, S) \to E_2(\tau, 0)$ for $\tau \to \infty$, are clearly visible in the three-dimensional plot.

So, the second harmonic generation in an optical fiber terminates on reaching the equilibrium state. Despite the fact that there exists a strong static field $[E_0(\tau, S) = 1]$ satisfying the phase-matching condition $\varkappa = k_{2\omega} - 2k_\omega$, the second harmonic generation does not occur in the stationary state, which exemplifies a destructive wave interference. To resume the generation after its self-termination, the established equilibrium should be disturbed, which can be accomplished by changing the phase of the prime second-harmonic wave or its amplitude. Figure 17 shows the self-termination process and an active generation burst following a change of the phase of the prime wave. A similar burst is also observed upon changing the wave amplitude.

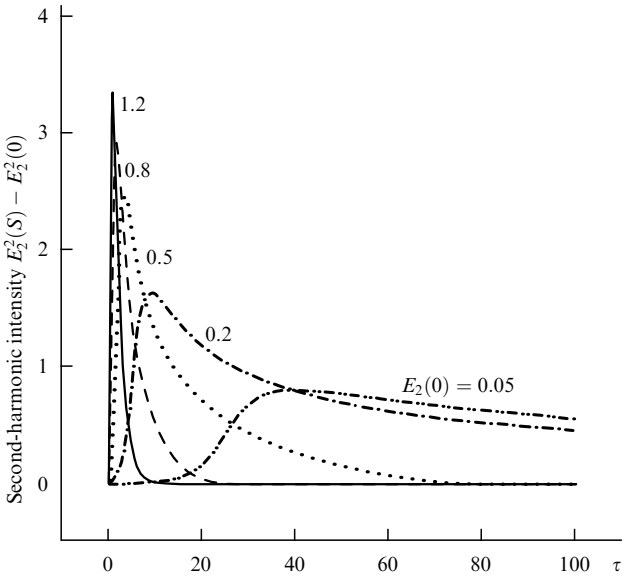

Figure 15. Time dependences of the output second-harmonic signal for different amplitudes of the input signal $E_2(0)$.

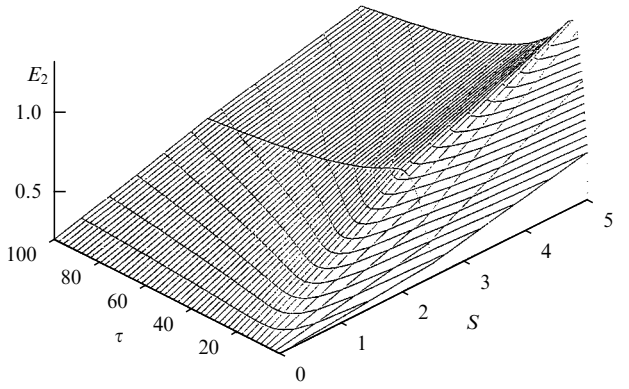

Figure 16. Amplitude growth of the second-harmonic field E_2 at the preparation stage and generation termination in a completely prepared state for $E_2(0) = 0.2$, $E_0(0) = 0$, and $\psi_0(0) = \psi_2(0) = 0$.

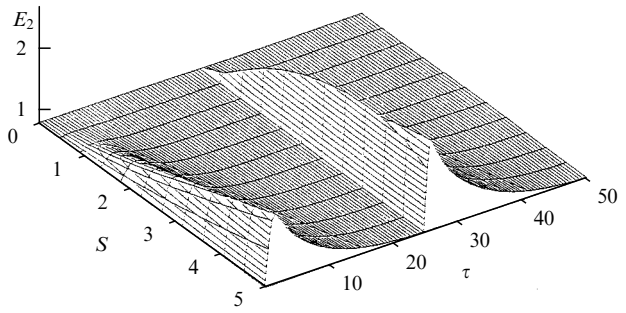

Figure 17. Amplitude of the second-harmonic signal for the initial conditions $E_2(0, \tau) = 0.8$, $E_0(S, 0) = 0$, $\psi_0(0) = \psi_2(0) = 0$ and its response to a phase change $\Delta\psi_2 = \pi$ for $\tau = 25$.

4.2 Highly efficient second harmonic generation

We now direct our attention to the more general case, not imposing any limitations on the first-to-second harmonic amplitude ratio [26]. In this situation we can no more disregard the variations of the fundamental wave: in addition to the variations of the second harmonic and the static field considered in Section 4.1, we should investigate the variation of the amplitude and the phase of the first harmonic too.

The fields of the static polarization, the first and second harmonics will be sought in the form

$$E_{\rm dc}(z,t) = -A_0(z,t)\exp\left[\mathrm{i}(k_{2\omega} - 2k_\omega)z + \mathrm{i}\psi_0(z)\right],$$
$$E_\omega(z,t) = A_1(z)\exp\left[\mathrm{i}k_\omega z - \mathrm{i}\omega t + \mathrm{i}\psi_1(z)\right],$$
$$E_{2\omega}(z,t) = A_2(z)\exp\left[\mathrm{i}k_{2\omega}z - 2\mathrm{i}\omega t + \mathrm{i}\psi_2(z)\right], \qquad (4.6)$$

respectively. We substitute the expressions for the first and second harmonics (4.6) into the wave equation (4.1) to obtain the equations for the derivatives of their complex amplitudes:

$$\frac{\partial}{\partial z} A_1\left[\exp(\mathrm{i}\psi_1)\right] = \mathrm{i}\,\frac{2\pi\omega}{cn_\omega}\,P_\omega\,,$$
$$\frac{\partial}{\partial z} A_2\left[\exp(\mathrm{i}\psi_2)\right] = \mathrm{i}\,\frac{4\pi\omega}{cn_{2\omega}}\,P_{2\omega}\,. \qquad (4.7)$$

We supplement the system (4.7) with equations describing the response of the medium. The polarizations P_ω and $P_{2\omega}$ at the fundamental and doubled frequencies arise owing to the $\chi^{(3)}$ nonlinearity in the presence of a strong static electric field:

$$P_\omega = \chi^{(3)}E_{\rm dc}^* E_\omega^* E_{2\omega}\,, \quad P_{2\omega} = \chi^{(3)}E_{\rm dc}E_\omega^2\,.$$

The fundamental wave and the second harmonic by virtue of rectification produce a fast-response nonlinear polarization

$$P_{\rm dc}^{(0)} = \chi^{(3)}A_2A_1^2\exp\left[\mathrm{i}(k_{2\omega} - 2k_\omega)z + \mathrm{i}(\psi_2 - 2\psi_1)\right]$$

and a corresponding electric field

$$E_{\rm dc}^{(0)} = -4\pi q P_{\rm dc}^{(0)}\,,$$

which is phase-matched but weak in amplitude.

Under the action of pumping, the initial prime field is amplified through the CTEs and exponentially tends (retaining the phase memory) to saturation:

$$E_{\rm dc} \to -u \exp\left[\mathrm{i}(k_{2\omega} - 2k_{\omega})z + \mathrm{i}(\psi_2 - 2\psi_1)\right],$$

with a rate $\alpha_2 A_2^2$ proportional to the pump power. The corresponding equation for the passage of the static polarization field $E_{\rm dc}$ to saturation is of the form

$$\frac{\partial}{\partial t}\left[A_0 \exp(\mathrm{i}\psi_0)\right] = \alpha_2 A_2^2 \left[u \exp(\mathrm{i}\psi_2) - A_0 \exp(\mathrm{i}\psi_0)\right]. \quad (4.8)$$

The last equation for the static polarization field and the system of equations (4.7) for the fundamental wave and the doubled frequency wave make up a complete closed system, which governs the propagation and the interaction of the waves in the general case.

Like in Section 4.1, for the following investigation it is advantageous to introduce the dimensionless variables

$$E_0 = \frac{A_0}{u}, \quad E_1 = \frac{\sqrt{n_\omega} A_1}{u}, \quad E_2 = \frac{\sqrt{n_{2\omega}} A_2}{u},$$
$$S = \varkappa_0 z, \quad \varkappa_0 = \frac{4\pi\omega\chi^{(3)} A_1^2}{c n_\omega \sqrt{n_{2\omega}}}, \quad \tau = \alpha_2 u^2 t. \quad (4.9)$$

Separating the amplitudes and the phases in Eqns (4.7) and (4.8) leads us to a universal system of equations, which transforms to the system of equations (4.5) for $E_2/E_1 \ll 1$:

$$\begin{aligned}
&\frac{\partial E_2}{\partial S} = E_0 E_1^2 \sin(\psi_0 + 2\psi_1 - \psi_2),\\
&E_2 \frac{\partial \psi_2}{\partial S} = -E_0 E_1^2 \cos(\psi_0 + 2\psi_1 - \psi_2),\\
&\frac{\partial E_1}{\partial S} = -E_0 E_1 E_2 \sin(\psi_0 + 2\psi_1 - \psi_2),\\
&E_1 \frac{\partial \psi_1}{\partial S} = -E_0 E_1 E_2 \cos(\psi_0 + 2\psi_1 - \psi_2),\\
&\frac{\partial E_0}{\partial \tau} = -E_2^2\left[E_0 - \cos(\psi_0 + 2\psi_1 - \psi_2)\right],\\
&E_0 \frac{\partial \psi_0}{\partial \tau} = -E_2^2 \sin(\psi_0 + 2\psi_1 - \psi_2).
\end{aligned} \quad (4.10)$$

Like Eqns (4.5), the resultant system of equations has a stationary solution

$$E_0(\tau, S) = 1, \quad E_1(\tau, S) = E_1(0), \quad E_2(\tau, S) = E_2(0),$$
$$\psi_0 + 2\psi_1 - \psi_2 = 0,$$

where $E_1(0)$ and $E_2(0)$ are the field amplitudes of the input radiation, i.e. only the phases of the waves of the first and second harmonics vary, while the generation does not occur.

Figure 18 shows the numerical solution of the system of equations (4.10) for the initial conditions

$$E_0(\tau, S) = 0, \quad E_1(0) = 1, \quad E_2(0) = 0.05,$$
$$\psi_0(S, 0) = \psi_1(0) = \psi_2(0) = 0,$$

which correspond to an input power of the fundamental wave of 10^9 W/cm^2, and the second harmonic of 2×10^6 W/cm^2. The plot demonstrates the presence of highly efficient generation at the stage of optical-fiber preparation, the build-up of the second-harmonic amplitude, and the passage to the quasi-equilibrium state. The spatio–temporal oscillations of the system conclude with a transition to the completely prepared state, in which the wave amplitudes are invariable.

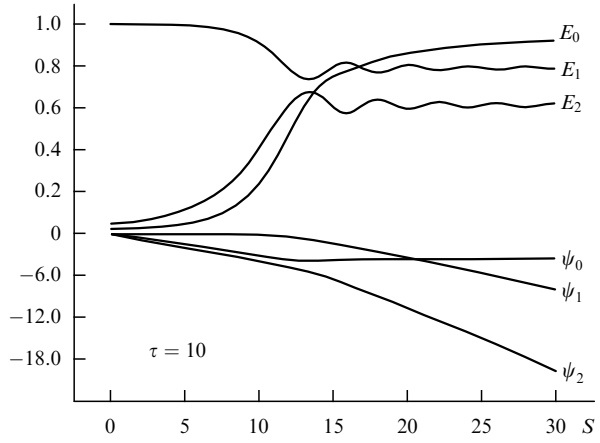

Figure 18. Spatial dependence of the amplitudes and the phases.

We also investigated the time dependence of the efficiency of frequency doubling, $f(S) = [E_2^2(S) - E_2^2(0)]/E_1^2(0)$. Since the radiation power in a dispersion medium is $cnA^2/4\pi$ (we note the factor cn and not c/n [19]), the efficiency $f(S)$ is the ratio of the gain in second-harmonic power to the power of the incident fundamental wave. The sought dependence for $S = 5$, $E_1(0) = 1$, and $E_2(0) = 0.3$ is represented by the lower curve in Fig. 19, which shows the rise and the subsequent decay of the generation efficiency.

A high-efficiency and stable frequency doubler can be obtained by varying the input wave parameters (the amplitude and/or the phase) in the required way. For instance, if the phase of the incident fundamental wave is monotonically changed by rotating a transmission phase shifter with a period T $\left(\psi_1(0) = 2\pi\tau/T\right)$, the efficiency becomes constant and close to 100%, as shown in Fig. 19 for different periods T of rotation of the transmission phase shifter. Changing the input beam parameters prevents the system from going over to the stationary (completely prepared) state and its attendant self-termination of generation. The result arrived at shows that, as in the case of frequency doubling by a nonlinear

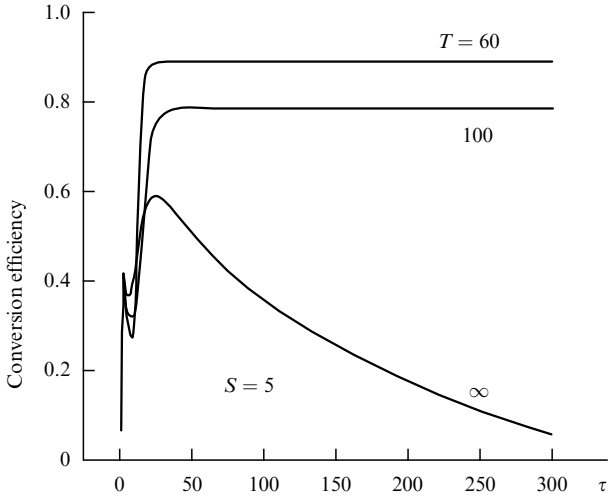

Figure 19. Efficiency of frequency doubling for different periods T of rotation of a transmission phase shifter.

crystal, there are no fundamental limitations on the conversion efficiency (technical ones, naturally, are bound to arise).

In the investigation of the energy transfer from the second harmonic wave to the fundamental wave (the inverse conversion), which occurs when the amplitude of the input second harmonic wave exceeds the amplitude of the first one, we discovered a behavior similar to the direct conversion considered above.

Therefore, in this section we obtained the systems of equations for the amplitudes and the phases of the fields of static polarization, the first and second harmonics, which describe the wave propagation in the optical fiber, and derived their solutions. The equations give the spatio–temporal scale in agreement with experiments and the values of the field amplitudes. Furthermore, they show that the second harmonic generation takes place at the preparation stage owing to a delay in the system response (the slowness of formation of static polarization). The generation self-switches off upon completion of the preparation. We have studied the conversion efficiency and proposed a mechanism of producing an efficient frequency doubler. The theory outlined is consistent with available experimental results and predicts new ones (see also Refs [25, 26]). A more comprehensive comparison of the theoretical findings with experiments is the subject matter of Section 5.

5. Comparison of the theory with experiments and the results of other models

As already noted in Section 4, the resultant systems of equations for the amplitudes and the phases of the fields of static polarization and the first- and second-harmonic waves (4.5) and (4.10) yield nontrivial scales of the quantities: the amplitude of the static electric field, $u \approx 10^5$ V/cm; the saturation length $\varkappa_0^{-1} \approx 10$ cm, and the characteristic time of the process, $(\alpha_2 u^2)^{-1} \approx 5$ min, which are in complete agreement with the experimental data [5, 8]. Also observed in experiments are the growth and the self-termination of generation. Moreover, in conformity with the theory, the rate of the process increases with increasing power of the input radiation, while the state prepared employing an extremely weak second harmonic [5] decays very slowly, so that it resembles the stationary one.

The experiments of Refs [27–29] were staged to investigate the phase difference between the second-harmonic wave generated and the prime wave. It turned out that the phase difference is $-\pi/2$ in a thin sample [25], while it is -71° [28] and 99° [29] in an extended sample.

The answer to the question of the significance of the sought phase difference is provided by an analysis of Eqn (4.2) with consideration for the direction of the field of resultant static polarization. We substitute the value of the static nonlinear polarization field in the formula for the amplitude of nonlinear polarization $P_{2\omega} = \chi^{(3)} E_{\rm dc} E_\omega^2$ at the doubled frequency. As shown in Section 4.1, the static field $E_{\rm dc}$ originates due to the CTE amplification of the prime field and tends to saturation:

$$E_{\rm dc} = -u \exp\left[\mathrm{i}(k_{2\omega} - 2k_\omega)z + \mathrm{i}\psi_2\right].$$

In view of this, from Eqn (4.2) we obtain

$$\frac{\partial}{\partial z}\left[A_2 \exp(\mathrm{i}\psi_2)\right] = -\mathrm{i}\,\frac{4\pi\omega\chi^{(3)} u A_1^2}{c n_{2\omega}} \exp(\mathrm{i}\psi_2), \qquad (5.1)$$

where A_1 is the amplitude of the fundamental wave field.

Equation (5.1) has a simple solution

$$A_2(z) = A_2(0), \quad \psi_2(z) = -kz,$$

where

$$k = \frac{4\pi\omega\chi^{(3)} u A_1^2}{c n_{2\omega} A_2} \approx 10^{-1}\ \text{cm}.$$

For a short sample ($kz \ll 1$), the complex amplitude of the second harmonic is

$$\begin{aligned} E_{2\omega} &= A_2(z)\exp(\mathrm{i}k_{2\omega}z - 2\mathrm{i}\omega t - \mathrm{i}kz) \\ &= A_2(z)\exp(\mathrm{i}k_{2\omega}z - 2\mathrm{i}\omega t)\,[1 - \mathrm{i}kz], \end{aligned}$$

i.e. the second harmonic is the sum of the prime wave

$$A_2(z)\exp(\mathrm{i}k_{2\omega}z - 2\mathrm{i}\omega t)$$

and the wave

$$\begin{aligned} &-\mathrm{i}kz\,A_2(z)\exp(\mathrm{i}k_{2\omega}z - 2\mathrm{i}\omega t) \\ &\quad \equiv kzA_2(z)\exp\left(\mathrm{i}k_{2\omega}z - 2\mathrm{i}\omega t - \mathrm{i}\frac{\pi}{2}\right), \end{aligned}$$

which results from the generation. One can see that the latter is shifted in phase by $-\pi/2$ relative to the prime wave, which is consistent with Ref. [25].

Of fundamental importance is the minus sign in the right-hand side of Eqn (5.1). It appears due to the positive feedback in the response to an external field (see Section 3). In the case of a thermodynamic response (the dipole moment originating in the medium is aligned with the acting field), the right-hand side of Eqn (5.1) changes sign and so does the phase shift. We note that a formula similar to Eqn (5.1) was obtained in Ref. [27], where the minus sign was introduced to reach agreement with the experiment. In an optical fiber of arbitrary length, a wave proportional to $\exp(\mathrm{i}k_{2\omega}z - 2\mathrm{i}\omega t - \mathrm{i}\pi/2)$ initiates a wave proportional to $\exp(\mathrm{i}k_{2\omega}z - 2\mathrm{i}\omega t - \mathrm{i}\pi)$, etc.

The general solution for the second-harmonic field can be represented as a superposition of four waves, with their phases shifted by $-\pi/2$ relative to each other:

$$\begin{aligned} E_{2\omega} &= A_2(0)\exp(\mathrm{i}k_{2\omega}z - 2\mathrm{i}\omega t - \mathrm{i}kz) \\ &= A_2(0)\exp(\mathrm{i}k_{2\omega}z - 2\mathrm{i}\omega t)\sum_{n=0}^{\infty}\frac{(-\mathrm{i}kz)^n}{n!} \\ &= A_2(0)\exp(\mathrm{i}k_{2\omega}z - 2\mathrm{i}\omega t)\left[\left(1 + \frac{(kz)^4}{4!} + \frac{(kz)^8}{8!} + \ldots\right)\right. \\ &\quad - \mathrm{i}\left(kz + \frac{(kz)^5}{5!} + \frac{(kz)^9}{9!} + \ldots\right) \\ &\quad - \left(\frac{(kz)^2}{2!} + \frac{(kz)^6}{6!} + \frac{(kz)^{10}}{10!}\ldots\right) \\ &\quad \left. + \mathrm{i}\left(\frac{(kz)^3}{3!} + \frac{(kz)^7}{7!} + \frac{(kz)^{11}}{11!}\ldots\right)\right] \\ &= A_2(0)\exp(\mathrm{i}k_{2\omega}z - 2\mathrm{i}\omega t)\left[\frac{\cosh(kz) + \cos(kz)}{2}\right. \\ &\quad + \exp\left(-\mathrm{i}\frac{\pi}{2}\right)\frac{\sinh(kz) + \sin(kz)}{2} \\ &\quad + \exp(-\mathrm{i}\pi)\frac{\cosh(kz) - \cos(kz)}{2} \\ &\quad \left. + \exp\left(-\mathrm{i}\frac{3\pi}{2}\right)\frac{\sinh(kz) - \sin(kz)}{2}\right]. \end{aligned}$$

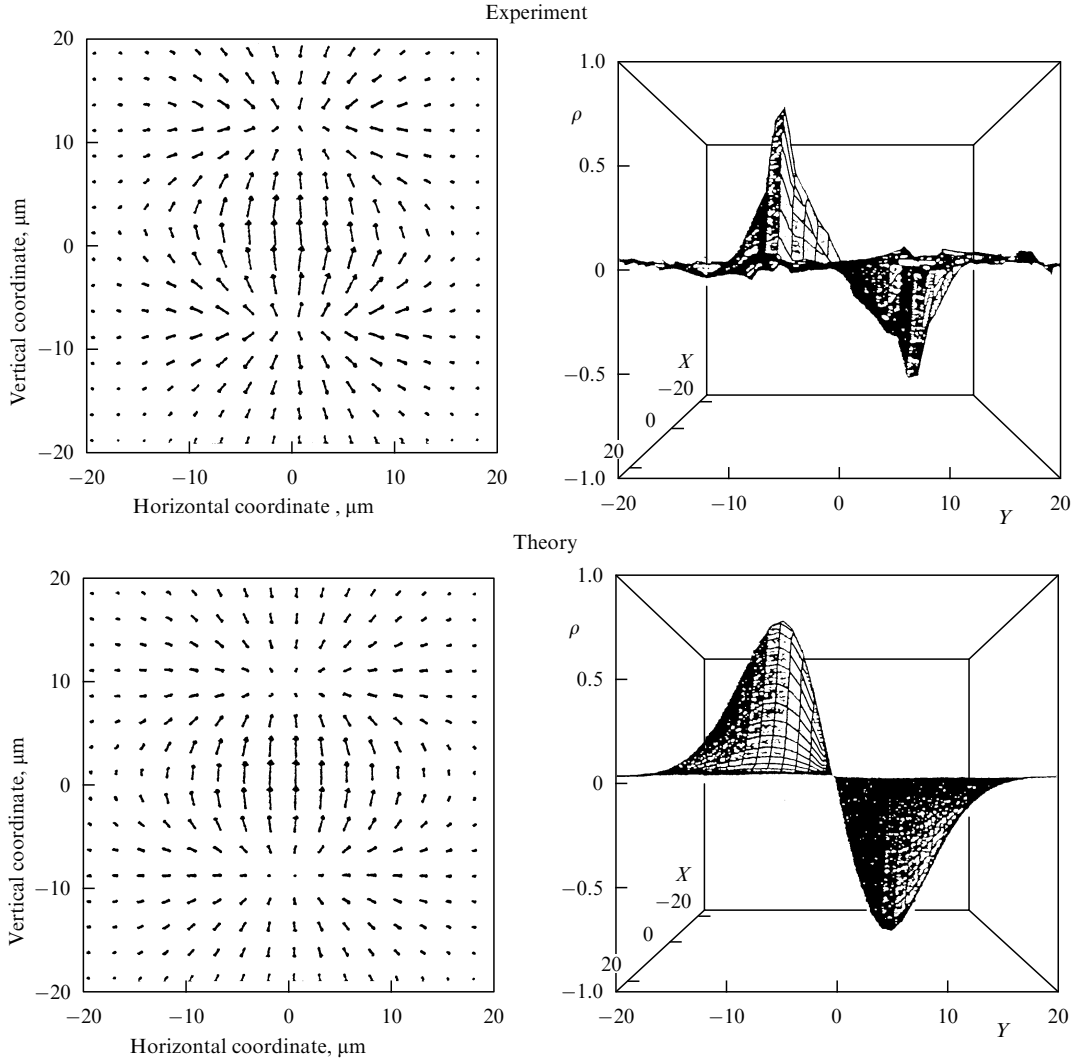

Figure 20. Distribution of the static field over the sample and the corresponding charge distribution [30].

The corresponding amplitudes vary along the optical fiber, and the resultant phase of the second-harmonic wave in an extended optical fiber can have any shift relative to the prime wave [28, 29].

Dominic and Feinberg [30] demonstrated the occurrence of a static polarization field E_{dc} in a sample and measured its distribution over the section of the sample (Fig. 20). The shape of this distribution is easily obtainable within the framework of the theoretical model outlined. The initial nonlinear static polarization of a sample is described by the formula $P_{dc}^{(0)} = \chi^{(3)} E_{2\omega} E_{\omega}^{*} E_{\omega}^{*}$ and is Gaussian along the lateral coordinates, since the field intensities in the laser beam are Gaussian in shape. Under the action of pumping, the CTEs strengthen the polarization, leaving, however, its shape invariable: $P_{dc}^{(0)} \to P_{dc}$. The strong static field originating in this way corresponds to the field of the charge distributed over the section with a density

$$\rho = -\mathrm{div}\, P_{dc} = -\frac{\partial}{\partial y} \exp\left(-\frac{x^2 + y^2}{d^2}\right), \qquad (5.2)$$

where d is the lateral beam dimension, i.e. E_{dc} corresponds to the field of a spatially spread dipole, which is in complete agreement with the experiment [28].

It is pertinent to note that the distance between the density peaks of positive and negative charges is $d \approx 10$ μm. This distance only corresponds to the scale of P_{dc} variation, but electrons are, on the average, transferred by microscopic distances $r \ll d$. Formula (5.2) was obtained by fitting the experimental data in Ref. [30]. Since E_{dc} changes sign in the vertical direction, shifting the radiation focal spot at the preparation stage yields different results for various shift directions [31]. If the shifting is accomplished in the vertical direction, each portion of the sample is, with the exception of the boundaries, polarized in turn in the opposite directions and the major part of the volume proves to be unprepared. If the shifting is accomplished in the horizontal direction, the repolarization does not take place and the sample proves to be prepared throughout the volume in accordance with Ref. [31].

Finally, an experimental study was recently made of the effect of a strong external static field E_{ext} on the efficiency of generation [32]. It was found that the imposition of a strong external electric field after the self-termination of generation brings about its burst followed by a decay (Fig. 21). And, which is by no means trivial, the removal of the external field after the self-retermination of generation results in a new burst of generation. Such a behavior is explicable on the basis of our theoretical model. As already noted, the frequency

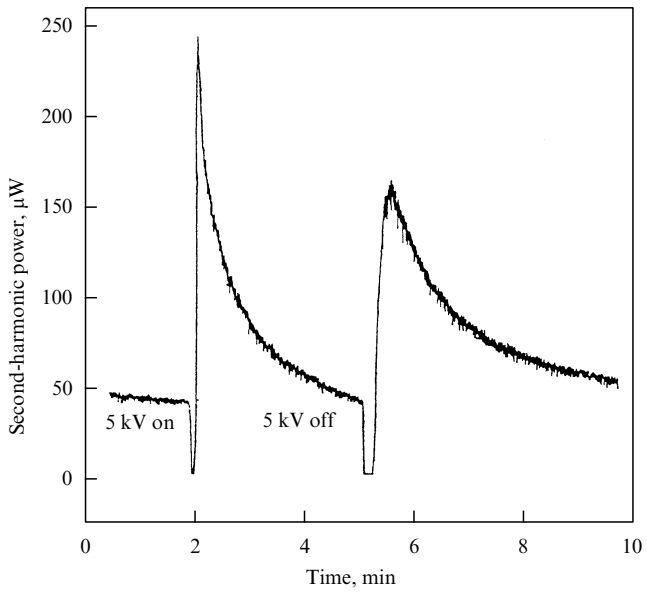

Figure 21. Bursts of second harmonic generation following the imposition and removal of an external electric field E_{ext} (experiments of Ref. [32]).

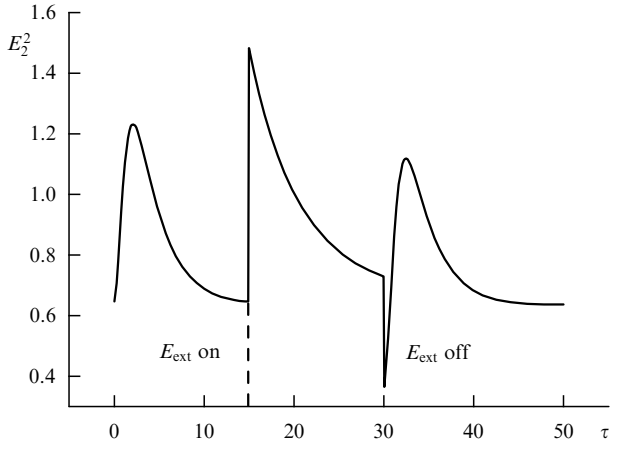

Figure 22. Effect of a strong external electric field E_{ext} on the intensity of the output second-harmonic signal for $E_2(0) = 0.8$, $\delta\varphi = 6S$, and $\eta = 0.15$ (theory).

doubling is only possible at the stage of the system transition to the equilibrium state and self-terminates when the system reaches it. Any 'shaking' of the system — be it the imposition or the removal of an external field — disturbs the equilibrium and results in the resumption of generation.

Let us investigate in greater detail the response of the system to the imposition or the removal of an external electric field E_{ext}. A strong external field ($d_0 E_{\text{ext}}/\Delta \approx 100 \gg 1$) shifts the energy levels far away from resonance [see formula (3.1) and Fig. 9] and the Ge-centers become inactive. The existing field decays owing to the recombination of electrons and holes, and the amplification of the initial field $E_{\text{dc}}^{(0)}$ terminates. In addition to varying E_{dc}, the external field introduces an additional phase shift between the first- and second-harmonic waves

$$\delta\psi = \frac{2\omega}{c}\left(\chi^{(3)}(\omega,0,0) - \chi^{(3)}(2\omega,0,0)\right) E_{\text{ext}}^2\, z \equiv \xi S\,,$$

where $\xi \approx 6$ for the experimental values $E_{\text{ext}} = 10^7$ V/cm, and $\chi^{(3)} = 10^{-14}$ esu.

We found the sought response of the system to a strong external field with the aid of the system of equations (4.5), assuming that at the instant of imposition of E_{ext} an exponential decay of the polarization field amplitude $[E_0(\tau, S) = E_0(S)\exp(-\eta\tau)]$ commences and an additional phase difference $\delta\psi = \xi S$ appears. It was found that both the imposition and the removal of a strong external field E_{ext} result, in complete agreement with experiments, in a burst of the second-harmonic signal (Fig. 22).

Therefore, the implications of the theoretical model are in complete agreement with the available experimental data. The theory also predicts new interesting results, for instance, the feasibility of producing a stable high-efficiency frequency doubler (see Section 4.2).

Several other theories have been proposed, which have served the purpose of describing the self-organization of excitations in silica optical fibers [9 – 12, 33]. Regrettably, all of them came to a halt at the stage of construction of the system response (construction of material relationships), while the description of experiments would remain at a qualitative level.

All the theories, with the exception of ours, invoke the multiphoton absorption of the first- and second-harmonic photons: a combination of the ω- and 2ω-photons, which results in the production of free electron and hole states in glasses (Refs [9 – 12]), and local electron states excited by the fourth harmonic 4ω (Ref. [33]). Our theory invokes only local electron and hole states and no more than single-photon processes (the absorption of one photon of the second harmonic).

Linear and nonlinear processes are easy to distinguish experimentally. In our theory, the prime static field E_0 is induced by the rectification of the first- and second-harmonic fields: $E_0 \propto E_{2\omega}^2 E_\omega$. It is of importance only at the initial stage of instability development. Once the ordered state has commenced setting in, the static field E_0 can be removed (by switching off one of the light fields), while the formation process would, of course, continue (for details, see Ref. [25]).

In the theories of Refs [9 – 12], the current $J \propto E_{2\omega}^2 E_\omega$ that forms the state exists only under the simultaneous action of the first and second harmonics throughout the process and vanishes on turning down one of the fields (the preparation of the state discontinues). This circumstance makes it possible to experimentally elucidate the question of what mechanism is realized in silicate glasses. The answer to this question was provided in a recent experiment [34, 35].

The first and second harmonics of a pulsed Nd : YAG laser were focused in a silicate PM-4 plate (K-8 glass), a long-lived grating was written whose amplitude was monitored by diffraction and the efficiency of second harmonic generation. The preparation of the state was initiated by two waves: the fundamental ω and the second harmonic 2ω; then, one of them was shut off. In this case, it was found that one wave (the fundamental or the second harmonic) continues the state preparation. In the case when only the fundamental wave is introduced, the interpretation is less clear, because the grating doubles the ω frequency and both waves, ω and 2ω, act on the sample.

The interpretation of the experiment with the second harmonic is evident. The two waves commence the preparation of a grating with a wave vector $\mathbf{K} = \mathbf{k}_{2\omega} - 2\mathbf{k}_\omega$ (the statement is valid for all the theories [9 – 12, 15, 23, 24]). In

our theory, **K** is the wavevector of the rectified electric field $E_0 = -4\pi q\chi^{(3)}E_{2\omega}^2 E_\omega^*$, the initial field E_0 is amplified by one wave, whereas in Refs [9–12] the state is prepared only by the simultaneous action of the two waves. According to experiments, the second harmonic continues the writing on turning off the fundamental wave, as shown in Fig. 23 borrowed from Refs [34, 35].

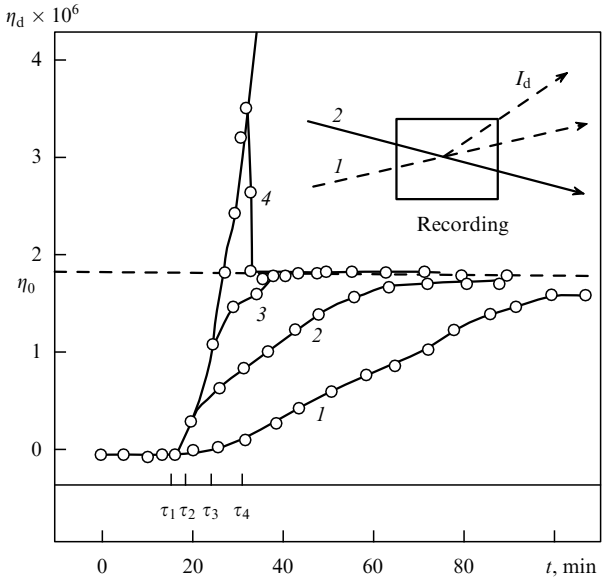

Figure 23. Time dependence of the diffraction efficiency of the fundamental wave for different durations of two-wave preparation: $\tau_1 = 16$ min, $\tau_2 = 20$ min, $\tau_3 = 25$ min, and $\tau_4 = 32$ min. Curves *1–4* correspond to the specified values of τ_i (experiments of Refs [34, 35]).

Irrespective of the way of preparation, one and the same grating amplitude is accomplished. However, the saturation level is higher with the action of two waves, and therefore the upper curve falls off. When a 2ω wave is introduced into the sample, the grating does not generate the ω wave. The possible 4ω harmonic can, according to Refs [9–12], in general write down another grating with a wavevector $\mathbf{K}^* = \mathbf{k}_{4\omega} - 2\mathbf{k}_{2\omega}$ and not the **K** grating. What is more, the 4ω wave is strongly absorbed in silicate glass and can hardly play a significant part for this reason. Therefore, the results given in Fig. 23 suggest that our model is realized in silicate glass rather than the model of Refs [9–12, 33].

6. Conclusions

The experiments conducted and the analysis of the experimental data of Refs [15–17] lead us to conclude that a new type of excitation arises in a silica optical fiber on addition of the GeO_2 dopant — charge transfer excitons. On absorption of one photon of green light, an electron transfers from an impurity Ge-center to the matrix or a different Ge-center. A CTE is localized in space and has a static dipole moment; because the electron and the hole are spatially separated, this type of excitation is long-lived. An original theoretical model involving the CTEs was elaborated, which describes the second harmonic generation in Ge-doped silica optical fibers.

The results presented in the foregoing disclose that a self-organization occurs (orientation ordering of dipole moments) owing to the interaction of the dipole moments in the system of CTEs. In this case, a positive feedback is formed in the system in response to a weak prime electric field: the CTEs are so excited that their dipole moments are primarily directed in opposition to the field and the resultant polarization strengthens this field. The system reaches its saturation when the amplitude of the emergent strong static field attains a value of $10^5 - 10^7$ V/cm. This field breaks the inversion symmetry initially existing in the volume of the optical fiber and makes possible the efficient generation of the second harmonic.

The investigation of wave propagation in a Ge-doped silica optical fiber taking into account the interaction of waves with CTEs allowed us to derive the systems of equations for the amplitudes and the phases of the fields of static polarization, the first and the second harmonic and find their solutions. The equations provide a complete description of the wave propagation through the optical fiber. The second harmonic generation takes place at the preparation stage owing to a time lag in the system response (the slowness of the formation of static polarization). Upon completion of the preparation, the generation self-switches off.

Calculating the spatial and temporal scales of self-organization has made it possible to find the phase relations between the resultant second-harmonic wave and the prime wave and the distribution of the emergent static field over the section. Both the imposition and the removal of an external electric field result in bursts of second harmonic generation.

The theory outlined above is consistent with the known experimental results and predicts new ones. It furnishes a possibility of producing a high-efficiency frequency doubler and purely optical poling (polarization induction) in glasses.

This work was performed under the auspices of the Ministry of Industry, Science, and Technology of the Russian Federation (Grant No. 08.02.16) and the Russian Foundation for Basic Research (Grant No. 00-02-16051).

References

1. Zaikin A N, Zhabotinskii A M *Nature* **225** 535 (1970)
2. Benard H *Rev. Gen. Sci. Pures Appl.* **12** 1261 (1900)
3. Turing A M *Philos. Trans. Roy. Soc. B* **237** 37 (1952)
4. Arecchi F T *Physica D* **86** 297 (1995)
5. Osterberg U, Margulis W *Opt. Lett.* **11** 516 (1986)
6. Fujii Y et al. *Opt. Lett.* **5** 48 (1980)
7. Podobedov V B *J. Raman Spectrosc.* **27** 731 (1996)
8. Stolen Q H, Tom H W K *Opt. Lett.* **12** 585 (1987)
9. Dianov E M, Kazanskiĭ P G, Stepanov D Yu *Kvantovaya Elektron.* (Moscow) **16** 887 (1989) [*Sov. J. Quantum Electron.* **19** (5) 575 (1989)]
10. Dianov E M, Starodubov D S *Opt. Fiber Technol.* **1** (1) 3 (1994)
11. Baranova N B, Chudinov A N, Zel'dovich B Ya *Opt. Commun.* **79** 116 (1990)
12. Anderson D Z, Mizrahi V, Sipe J E *Opt. Lett.* **16** 796 (1991)
13. Antonyuk B P *Fiz. Tverd. Tela* (Leningrad) **28** 3624 (1986)
14. Neustruev V B et al. *Fiber Integrated Opt.* **8** 143 (1989)
15. Antonyuk B P et al. *Phys. Lett. A* **213** 297 (1996)
16. Antonyuk B P, Denisov V N, Mavrin B N *Pis'ma Zh. Eksp. Teor. Fiz.* **68** 737 (1998) [*JETP Lett.* **68** 775 (1998)]
17. Antonyuk B P, Antonyuk V B, Frolov A A *Opt. Commun.* **174** 427 (2000)
18. Dianov E M et al. *Opt. Lett.* **22** 221 (1997)
19. Landau L D, Lifshitz E M, Pitaevskii L P *Elektrodinamika Sploshnykh Sred* (Electrodynamics of Continuous Media) (Moscow: Nauka, 1982) [Translated into English: 2nd ed. (Oxford: Pergamon Press, 1984)]
20. Antonyuk B P, Antonyuk V B *Phys. Lett. A* **249** 113 (1998)
21. Antonyuk B P, Antonyuk V B *J. Mod. Opt.* **48** 573 (2001)
22. Abakumov V N, Perel V I, Yassievich I N *Nonradiative Recombination in Semiconductors* (Modern Problems in Condensed Matter

Sciences, Vol. 33, Eds V M Agranovich, A A Maradudin) (Amsterdam: North-Holland, 1991)
23. Antonyuk B P, Musichenko S F *Phys. Scripta* **58** 83 (1998)
24. Antonyuk B P *Opt. Commun.* **181** 191 (2000)
25. Antonyuk B P, Antonyuk V B *J. Mod. Opt.* **45** 257 (1998)
26. Antonyuk B P, Antonyuk V B *Opt. Commun.* **147** 143 (1998)
27. Dominic V, Lambelet P, Feinberg J *Opt. Lett.* **20** 444 (1995)
28. Lambelet P, Feinberg J *Opt. Lett.* **21** 925 (1996)
29. Margulis W, Carvalho C S, von der Weid J P *Opt. Lett.* **14** 700 (1989)
30. Dominic V, Feinberg J *J. Opt. Soc. Am. B* **11** 2016 (1994)
31. Dianov E M et al. *Sov. Lightwave Commun.* **2** 83 (1992)
32. Kazansky P G, Pruneri V *Phys. Rev. Lett.* **78** 2956 (1997)
33. Lesche B *J. Opt. Soc. Am. B* **7** 53 (1990)
34. Balakirev M K *Phys. Vibrations* **6** 233 (1998)
35. Balakirev M K, Vostrikova L I, Smirnov V A *Pis'ma Zh. Eksp. Teor. Fiz.* **66** 771 (1997) [*JETP Lett.* **66** 809 (1997)]